

RADIATIVE-CONVECTIVE MODEL FOR ONE-DIMENSIONAL CLOUDY
SKY ATMOSPHERE

A THESIS SUBMITTED TO
THE GRADUATE SCHOOL OF NATURAL AND APPLIED SCIENCES
OF
MIDDLE EAST TECHNICAL UNIVERSITY

BY

MEHMET YUSUF KAPTAN

IN PARTIAL FULFILLMENT OF THE REQUIREMENTS
FOR
THE DEGREE OF MASTER OF SCIENCE
IN
CHEMICAL ENGINEERING

FEBRUARY 2011

Approval of the thesis:

**RADIATIVE-CONVETIVE MODEL FOR ONE-DIMENSIONAL CLOUDY
SKY ATMOSPHERE**

submitted by **MEHMET YUSUF KAPTAN** in partial fulfillment of the requirements for the degree of **Master of Science in Chemical Engineering Department, Middle East Technical University** by,

Prof. Dr. Canan Özgen
Dean, Graduate School of **Natural and Applied Sciences**

Prof. Dr. Deniz Üner
Head of Department, **Chemical Engineering**

Prof. Dr. Nevin Selçuk
Supervisor, **Chemical Engineering Dept., METU**

Assist. Prof. Dr. Görkem Külah
Co-Supervisor, **Chemical Engineering Dept., METU**

Examining Committee Members:

Assist. Prof. Dr. Tuba Okutucu Özyurt
Mechanical Engineering Dept., METU

Prof. Dr. Nevin Selçuk
Chemical Engineering Dept., METU

Assist. Prof. Dr. Nimeti Döner
Mechanical Engineering Dept., DPU

Assist. Prof. Dr. Görkem Külah
Chemical Engineering Dept., METU

Dr. Ahmet Bilge Uygur
Turkish Aerospace Industries, Inc.

Date: 11.02.2011

I hereby declare that all information in this document has been obtained and presented in accordance with academic rules and ethical conduct. I also declare that, as required by these rules and conduct, I have fully cited and referenced all material and results that are not original to this work.

Name, Last name: Mehmet Yusuf Kaptan

Signature :

ABSTRACT

RADIATIVE-CONVECTIVE MODEL FOR ONE-DIMENSIONAL CLOUDY SKY ATMOSPHERE

Kaptan, Mehmet Yusuf

M.Sc., Department of Chemical Engineering

Supervisor : Prof. Dr. Nevin Selçuk

Co-Supervisor: Asst. Prof. Dr. Görkem Külah

February 2011, 58 pages

Recent emphasis on the prediction of temperature and concentration fields in the atmosphere has led to the investigation of accurate solution methods of the time-dependent conservation equations for mass, momentum, energy and species. Atmospheric radiation is the key component of this system. Therefore, atmospheric radiation models were developed in isolation from the climate models.

The time-dependent multi-dimensional governing equations of atmospheric models must be solved in conjunction with the radiative transfer equation for accurate modeling of the atmosphere. In order to achieve this objective, a 1-D Radiative-Convective Model for Earth-Atmosphere System (RCM4EAS) was developed for clear and cloudy sky atmospheres. The radiative component of the code is Santa Barbara DISORT (Discrete Ordinate Radiative Transfer) Atmospheric Radiative Transfer (SBDART) integrated with exponential sum-fitting method as the radiative property estimation technique.

The accuracy of SBDART was tested by comparing its predictions of radiative fluxes with those of Line-by-Line Radiative Transfer Model (LBLRTM) for 1-D longwave (3.33-100 μm) clear sky atmosphere and a good agreement was obtained.

A parametric study aiming at finding the optimum parameters to be used as input in SBDART regarding the wavelength increment and order of approximation was also carried out. Variable wavelength and eight streams were selected as optimum parameters for the accuracy and computational efficiency.

The code was then coupled with a 1-D Radiative-Convective Model (RCM) to obtain the time dependent code, (RCM4EAS), which was applied to the investigation of the sensitivity of climate to changes in the CO₂ concentration for clear and cloudy sky conditions.

CO₂ sensitivity analyses revealed that doubling the CO₂ concentration in the earth's atmosphere from its present value (387 ppm) results in an increase in equilibrium surface temperature of 4.2 K in the clear sky atmosphere as opposed to 2.1 K in cloudy sky atmosphere with typical cloud physical parameters. It is worth noting that times required to reach equilibrium surface temperatures are approximately 2000 and 6000 days for clear and cloudy sky atmospheres, respectively and these temperature increases are calculated assuming that all the other parameters except CO₂ concentration remain unchanged within these time periods. Therefore, it should be noted that these temperature increases reflect only the effect of CO₂ doubling and excludes the effect of other forcings which might positively or negatively affect these temperature increases.

Overall evaluation of the performance of the code developed in this thesis study indicates that it can be used with confidence in 1-D radiative-convective modeling of the earth-atmosphere systems.

Keywords: Radiative-Convective Model, Atmospheric Radiation, Discrete Ordinates Method, Carbon Dioxide, SBDART.

ÖZ

BİR BOYUTLU, BULUTLU ATMOSFER İÇİN IŞINIM-TAŞINIM MODELİ

Kaptan, Mehmet Yusuf

Yüksek Lisans, Kimya Mühendisliği Bölümü

Tez Yöneticisi : Prof. Dr. Nevin Selçuk

Ortak Tez Yöneticisi: Yrd. Doç. Dr. Görkem Külah

Şubat 2011, 58 Sayfa

Atmosfer koşullarında sıcaklık ve konsantrasyon dağılımlarının tahmin edilmesine duyulan giderek artan gereksinim; zamana bağlı kütle, devinirlik, enerji ve madde korunum denklemlerinin çözümünü gerçekleştirecek yöntemlerin geliştirilmesini gerektirmiştir. Atmosferik ışınım çözümü gerçekleştirilecek sistemler bütününe en temel unsurdur. Bundan dolayı atmosferik ışınım modelleri iklim modellerinden ayrı olarak geliştirilmiştir.

Atmosferin doğru modellenmesi ortamın ışınım özelliklerinin güvenilir değerlendirilmesini ve atmosferik modellerin zamana bağlı çok boyutlu problemi tanımlayan denklemlerle birlikte ışınım ısı transfer denkleminin doğru çözülmesini gerektirmektedir. Bu amaca ulaşmak için yerküre-atmosfer sisteminin bulutsuz ve bulutlu atmosfer için bir boyutlu ışınım-taşınım modeli geliştirilmiştir. Geliştirilen kodun ışınım kısmı Santa Barbara DISORT (Belirli Yönler Yöntemi Işınım Transferi) Atmosferik Işınım Transferi (SBDART) yöntemine entegre edilmiş toplam eksponentli ışınım özellikleri hesaplama yönteminden oluşturulmuştur.

SBDART'ın öngörülerinin doğruluğu bulutsuz 1-Boyutlu atmosferde uzun dalga boyu aralığında (3.33-100 μ m) LBLRTM'in çözümleri ile karşılaştırılarak belirlenmiştir. SBDART'ın çözümlerinin öngörme doğruluğu ve hesaplama zamanı açısından optimize edilmesi için program değişik dalga boyu aralıkları ve akı sayısı için çalıştırılmış ve en uygun dalga boyu aralığının değişken dalga boyu aralığı, akı sayısının ise sekiz olduğu sonucuna varılmıştır.

Daha sonra SBDART ışınım-taşınım modeli ile birleştirilmiş ve kodun bulutsuz ve bulutlu atmosferde CO₂ konsantrasyonunun değişimine iklimin hassasiyeti incelenmiştir.

CO₂ konsantrasyonunun bugünkü değerinden (387 ppm) iki katına çıkarılması durumunda yerküre yüzey denge sıcaklığı artışının bulutsuz ortamda 4.2 K, bulutlu ortamda ise 2.1 K olduğu sonucuna varılmıştır. Yerküre yüzey denge sıcaklığı'na ulaşmak için bulutsuz ve bulutlu atmosfer koşullarında geçen süre sırasıyla yaklaşık olarak 2000 ve 6000 gündür. Bahsi geçen sıcaklık artışları bu süreçler içinde yalnızca CO₂ konsantrasyonundaki artış göze alınarak elde edilmiş, iklim değişikliği üzerinde sıcaklık artışı artırıcı ya da azaltıcı etke yapabilecek diğer etkenlerin değişmediği varsayılmıştır.

Bu tez çalışmasında geliştirilen kodun değerlendirilmesi sonucunda, kodun, yerküre-atmosfer sisteminin 1-boyutlu ışınım-taşınım modellenmesi için güvenle kullanılabileceğini göstermiştir.

Anahtar kelimeler: Işınım-Taşınım Modeli, Atmosferik Işınım, Belirli Yönler Yöntemi, Karbon Dioksit, SBDART.

To My Dearest Family

ACKNOWLEDGEMENTS

I wish to express my deepest gratitude to my supervisor, Prof. Dr. Nevin Selçuk for her guidance and encouragement throughout this study.

I would like to show my appreciation to my co-supervisor, Assist. Prof. Dr. Görkem Külâh, for her precious discussions and comments during the progress of this thesis.

I thank to the research team members for their friendship and support during my study; Güzide Sözen, İlker Soner, Mert Özkan and Nur Sena Yüzbaşı.

I would like to thank to the members of my dearest family Sacide, Enis, Zeynep, Neslihan, Kasım and my grandmother for their encouragement and motivation during this study.

Special thanks to my beloved father and grandfather who cannot share this moment with me.

This study was supported by The Scientific and Technological Research Council of Turkey (TÜBİTAK) Grant No: MAG-108M435.

TABLE OF CONTENTS

ABSTRACT.....	iv
ÖZ.....	vi
ACKNOWLEDGEMENTS.....	ix
TABLE OF CONTENTS.....	x
LIST OF TABLES.....	xii
LIST OF FIGURES.....	xiii
LIST OF SYMBOLS.....	xiv
CHAPTERS	
1. INTRODUCTION	1
2. SANTA BARBARA DISORT RADIATIVE TRANSFER CODE (SBDART)	5
2.1 Cloud Model	5
2.2 Gas Absorption Model.....	6
2.3 Radiative Transfer Equation Solver	7
2.4 Extraterrestrial Source Spectra.....	7
3. RADIATIVE-CONVECTIVE MODEL, RADIATION MODEL AND NUMERICAL SOLUTION PROCEDURE.....	8
3.1 Radiative-Convective Model.....	8
3.1.1 Description of the Model and Input Parameters	9
3.1.2 Estimation of Radiative Atmospheric Temperatures	13
3.1.2.1 Solar Heating Rates in the Atmosphere	14
3.1.2.2 Infrared Cooling Rates in the Atmosphere.....	15
3.1.2.3 Net Rate of Temperature Changes in the Atmosphere.....	15

3.1.2.4 Heating Rate in the Ocean Layer	16
3.1.3 Convective Adjustment	17
3.2 Radiation Model.....	19
3.2.1 The Radiative Transfer Equation (RTE).....	19
3.2.2 Discrete Ordinates Method (DOM).....	23
3.2.2.1 Angular Quadrature Scheme of DOM.....	26
3.2.3 Radiative Property Estimation Technique: Exponential-Sum Fitting	29
3.3 Numerical Solution Procedure.....	31
3.3.1 Algorithm of the code RCM4EAS	33
4. RESULTS AND DISCUSSION.....	37
4.1 Benchmarking SBDART against LBLRTM.....	38
4.2 Effect of Wavelength Increment on Computational Efficiency and Accuracy of SBDART	39
4.3 Effect of Number of Streams on Computational Efficiency and Accuracy of SBDART	40
4.4 Effect of Presence of Cloud and CO ₂ Concentration on Temperatures	41
4.5 Comparison of Predictions by RCM4EAS and Literature	47
5. CONCLUSIONS	48
REFERENCES	50
APPENDICES	
A. UTILIZATION OF LEGENDRE POLYNOMIALS IN RADIATIVE TRANSFER CALCULATIONS.....	53
B. NUMERICAL SOLUTION PROCEDURE OF DISCRETIZED RTE.....	56

LIST OF TABLES

TABLES

Table 3.1 Various atmospheric absorbers and corresponding mixing ratios in ppm..	10
Table 3.2 Direction cosines and weights specified by order of approximation.	28
Table 4.1 Effect of wavelength increment (wl) on net fluxes for clear sky.....	39
Table 4.2 Effect of wavelength increment (wl) on net fluxes for cloudy sky.....	40
Table 4.3 Effect of number of streams (Nstr) on net fluxes for clear sky	41
Table 4.4 Effect of number of streams (Nstr) on net fluxes for cloudy sky	41

LIST OF FIGURES

FIGURES

Figure 3.1 Schematic representation of plane-parallel atmosphere.....	9
Figure 3.2 Model input Temperature profile.....	12
Figure 3.3 Model input O ₃ concentration profile	12
Figure 3.4 Schematic representation of fluxes used in the model.....	13
Figure 3.5 Transfer of intensity from below in plane-parallel layers	20
Figure 3.6 Schematic drawing and geometry of plane-parallel atmosphere.....	21
Figure 3.7 Schematic representation of the multilayered medium.....	25
Figure 3.8 Flowchart of the coupled code.....	32
Figure 4.1 Comparison of net fluxes obtained by using LBLRTM and SBDART throughout the atmosphere	38
Figure 4.2 Surface temperatures with respect to time for different time increments and ocean layer depths in clear sky.....	42
Figure 4.3 Surface temperatures with respect to time in clear sky.....	43
Figure 4.4 Surface temperatures with respect to time for different time increments in cloudy sky	44
Figure 4.5 Surface temperatures with respect to time in cloudy sky.....	45
Figure 4.6 Equilibrium temperature profiles of clear and cloudy sky atmospheres...	46

LIST OF SYMBOLS

C_p	specific heat, [kJ/kgK]
C_{ij}	coefficients, [-]
F_{down}^S	downward solar flux, [W/m ²]
F_{up}^S	upward solar flux, [W/m ²]
F_{down}^{IR}	downward infrared flux, [W/m ²]
F_{up}^{IR}	upward infrared flux, [W/m ²]
F_{net}^S	net solar flux, [W/m ²]
F_{net}^{IR}	net infrared flux, [W/m ²]
g	acceleration due to gravity, [m/s ²]
h	ocean layer depth, [m]
I	radiative intensity, [W/m ² sr]
k	absorption coefficient, [kJ/kg]
L	latent heat of evaporation, [kJ/kg]
m	discrete direction, [-]
MW	molecular weight, [g/gmol]

P	pressure, [atm]
P^{sat}	saturation pressure of water vapor, [atm]
R	gas constant, [Latm/molK]
t	time, [s];
T	temperature, [K]
$\Delta\lambda$	variable wave length increment, [μm]
w_m	quadrature weight for ordinate m , [-]
z	co-ordinate axis, [-]

Greek Symbols

α	absorptivity, [-]
ε	emissivity, [-]
ϕ	azimuthal angle, [rad]
ν	wave length, [μm]
μ	direction cosines, [-]
θ	polar angle, [rad]
ρ	density, [kg/m^3]
σ	Stefan-Boltzmann constant, $=5.67 \times 10^{-8}$ [$\text{W}/\text{m}^2 \text{K}^4$]
τ	optical depth, [-]

ω	single scattering albedo, [-]
Ω	direction of radiation intensity, [-]
$d\Omega$	solid angle, [-]

Superscripts and Subscripts

a	air
adj	adjusted value
b	black body, beam source
CN	convection
IR	infrared radiation
N	net change
S	solar radiation
t	print time
v	spectral variable
w	water

Abbreviations

1-D	one-dimensional
BC	boundary condition
CLR	critical lapse rate

DISORT	discrete ordinate radiative transfer
DOM	discrete ordinates method
EBM	energy balance model
ESFT	exponential sum fitting of transmission functions
GCM	general circulation model
IR	infra-red
LAP	lapse rate
LBLRTM	line-by-line radiative transfer model
LW	long wavelength
ODE	ordinary differential equation
PDE	partial differential equation
RCM	radiative-convective model
RCM4EAS	radiative-convective model for earth-atmosphere system
RTE	radiative transfer equation
SBDART	Santa Barbara DISORT radiative transfer
SW	short wavelength
TOA	top of the atmosphere

CHAPTER 1

INTRODUCTION

There is a growing concern about the global climate change that has been a major issue on the media and the political agenda for decades. Understanding the climate change requires the knowledge of the climate system components and investigation of interactions between these components.

Observation of mean and statistical deviations of weather used to measure the variability of the average state of the atmosphere over a period of time is defined as *the climate*. Interaction of the atmosphere with other parts of the climate system such as the oceans, ice, snow, and land are probable causes of climate change that may result from the natural variability and/or anthropogenic perturbations.

Changes in the solar constant due to sunspot activities, changes in the solar insolation distribution caused by the earth's orbit around the sun, and changes in atmospheric composition as a result of volcanic eruptions, also expressed as *external forcings*, are among the sources of natural variability while anthropogenic perturbations are associated with increases in greenhouse gases and manmade aerosols [1].

A detailed discussion of the climate change phenomenon and an overview of general issues related with the earth-atmosphere system and the climate can be found elsewhere [2].

Atmospheric radiation is the key component for understanding the earth's climate and climate change that is associated with the emitted radiation from the sun and the absorption of solar energy by the atmosphere and the surface, as well as of the emission of thermal infrared energy from the earth-atmosphere system. Regarding

the radiation processes in the atmosphere, spectra can be divided into two regions above and below about $5 \mu\text{m}$; *solar radiation* concentrated in shorter wavelengths and the *thermal infrared radiation* concentrated in longwave range since the overlap between them is relatively small [1].

Based on the satellite radiation budget experiments, about 30 % of the incoming solar radiation at the top of the atmosphere (TOA) is reflected while the remaining part is absorbed in the earth-atmosphere system [1].

Solar radiation absorbed in the earth-atmosphere system must be re-emitted to space so that the global equilibrium temperature of the earth-atmosphere system remains relatively stable as observed over a climatological time scale. The atmosphere loses radiative energy to space through thermal infrared (IR) emission which leads to cooling in the earth-atmosphere system.

Net radiation is downward at the surface as most of the globe shows according to some direct surface observations over land and the ocean so that there is a net radiative energy gain in the surface [1]. Net energy gain due to the net downward solar radiation (incoming downward minus reflected) and downward IR radiation results in temperature increase at the surface and the surface loses energy to atmosphere via thermal infrared emission.

In a global sense, there is a net gain of radiative energy at the surface since the downward radiation absorbed by the surface is greater than the emitted radiance from the surface. Energy surplus at the surface is balanced by the transport of sensible and latent heat fluxes out of the surface to maintain an overall heat balance. On the other hand, the atmosphere experiences a net radiative cooling due to radiative processes as a result of the fact that the net emitted radiance is greater than the net absorbed solar radiation in the atmospheric layers. As a part of the overall heat balance, energy deficit in the atmosphere is balanced by the latent heat of condensation released in the precipitation processes and by the convection of sensible heat from the underlying surface. Atmospheric motion regarding the transport of sensible and latent heat that is the part of the overall heat balance mentioned above is generally classified as convection [1].

The pure radiative equilibrium temperature of the upper troposphere and the earth's surface were found to be much lower than the observed value [3,4] and this was attributed to the disregard of convection in the computations. This led to the development of convective adjustment scheme [5] in a global climate model for the first time in which the effects of convection are included implicitly by assuming that convection maintains a critical temperature lapse rate, which is nearly 6.5 K/km [1], within the convective region [6].

Climate models can be categorized into mainly four according to their complexity from the simplest to the most sophisticated. Simplest climate models are the zero-dimensional or 1-box climate models that the atmosphere is assumed to be a box comprising atmospheric absorbers with uniform concentrations that may change in time [7].

One-dimensional (1-D) climate models are more complex than 1-box models that are classified into two groups; the surface Energy Balance Models (EBMs) and the Radiative-Convective Models (RCMs). In EBMs, latitude is used as the spatial dimension so that the equilibrium surface temperature is estimated as a function of latitude while in the RCMs; the vertical height is used as the only coordinate. Development of a 1-D RCM is the focus of this study.

Two-dimensional models that consider both latitude and height, and the three-dimensional general circulation models (GCMs) in which all three dimensions of the earth's atmosphere is considered follows the 1-D models in the order of increasing complexity. Any of these models can be either steady state or time dependent [7].

The time-dependent multi-dimensional governing equations of atmospheric models must be solved in conjunction with the radiative transfer equation for accurate modeling of the atmosphere.

One dimensional (1-D) radiation models based on the assumption of plane parallel atmosphere are among the simplest models which are frequently used to estimate the radiative fluxes in the earth-atmosphere system. Two-stream or Eddington's approximation is utilized by many general circulation and climate models in the parameterization of radiative transfer, analytical solutions of which can be derived to

achieve efficient computation that is critical for model simulations. Although this approach has been shown to be an accurate and efficient means for the calculation of infrared fluxes in cloudy conditions [8,9], its accuracy is less satisfactory for the calculation of solar flux transfer due to the strong anisotropic nature of the scattering phase function for cloud particles [1].

Discrete Ordinate Method (DOM) is a useful and powerful method [10] for the computation of radiation fields in an atmosphere containing absorbing-emitting-scattering medium.

Radiative-Convective Models utilizing DOM as their RTE solver can be safely used for estimation of radiation fields in cloudy atmospheres. Among these studies, Hu et al. [11] used DOM with a data set of exponential sum fitting of transmission functions (ESFT) which has a resolution of 20 cm^{-1} for terrestrial radiation and an irregular spectral resolution for solar radiation [12] with four atmospheric absorbers; H_2O , CO_2 , O_3 and O_2 .

SBDART (Santa Barbara DISORT Atmospheric Radiative Transfer) is also a radiation code based on DOM and ESFT. However, it is integrated with LOWTRAN-7 atmospheric transmission code [13] in which an extended range of radiatively active species (CH_4 , N_2O , N_2 , O_2 , CO , NH_3 , SO_2 , NO , HNO_3 and NO_2) are considered. In addition, it is embedded with full range of cloud characteristics. It is the most comprehensive publicly available radiation code today.

Therefore the objective of the present study has been the development of a 1-D radiative-convective code embedded with SBDART for clear and cloudy sky atmospheres and investigation of climate to changes in CO_2 concentration levels.

CHAPTER 2

SANTA BARBARA DISORT ATMOSPHERIC RADIATIVE TRANSFER CODE (SBDART)

SBDART (Santa Barbara DISORT Atmospheric Radiative Transfer) is a publically available FORTRAN based computer code designed for solution of satellite remote sensing and atmospheric energy budget studies related radiative transfer problems. Developed by the atmospheric science community over the past few decades, the program is based on a collection of highly developed and reliable physical models that were described in the foregoing discussions. The key components of the code and their features are given in the following sections of this chapter.

2.1 Cloud Model

Clouds play a major role for determination of the earth's climate via reflecting solar radiation back out to space on one hand and absorbing part of the infrared radiation emitted by the Earth and reradiating it back to the surface on the other [14].

The single scattering albedo, defined as the probability of a photon to be scattered rather than being absorbed, the asymmetry factor indicating the strength of forward scattering and the scattering efficiency of the cloud has to be known for radiative transfer calculations within cloudy sky atmosphere. An internal database of these parameters computed with a Mie scattering code [15] covering an effective radius range of 2 to 128 μm for clouds exist in SBDART.

Shown to provide good accuracy when applied to radiative flux calculations [16,17], the Henyey-Greenstein parameterization is used to represent the angular distribution of scattered photons.

2.2 Gas Absorption Model

SBDART make use of low resolution band models providing clear sky atmospheric transmission from 0 to 50000 cm^{-1} that were derived from detailed line-by-line calculations and degraded to 20 cm^{-1} resolution for use in LOWTRAN 7 atmospheric transmission code [13]. The effects of all radiatively active molecular species corresponding to a wavelength resolution of about 5 nm in the visible and about 200 nm in the thermal infrared in the earth's atmosphere (c.f. sec. 3.1.1) are included in these models [14].

It is assumed that the transmission functions to be used for solution of radiative transfer equation in SBDART follow Beer's Law which states that the decrease in the radiant intensity traversing a homogeneous extinction medium is in accord with the simple exponential function whose argument is the product of the mass extinction cross section and the path length [1]. The path length through a slab of material depends not only on the slab thickness, but also on the amount of material in the slab. For Beer's Law to be valid, the incident radiation should preferably be monochromatic, or have at least a width that is narrower than the absorbing transition. Since the band models used in SBDART represent rather large wavelength bands, the transmission function for a given wavelength interval, $\Delta\nu$, has to be expressed as the sum of several exponential functions [18]. A three-term exponential fit adopted from LOWTRAN-7 is used in SBDART that a separate solution of the radiation transfer equation is implied in each term in the exponential fit (c.f. sec. 3.2.3). Since radiative transfer equation has to be solved only three times for each spectral interval, compared to a higher order fitting polynomials a great computational economy is achieved [14].

2.3 Radiative Transfer Equation Solver

In SBDART, DISORT routine (DIScret Ordinate Radiative Transfer) developed by Stamnes et al. [19] is used to integrate the radiative transfer equation numerically.

DISORT employs the discrete ordinate method (DOM) (c.f. sec. 3.2.2) which provides a numerically stable algorithm to solve the equations of plane-parallel radiative transfer in a vertically inhomogeneous atmosphere.

SBDART can be used to calculate the intensity of both scattered and thermally emitted radiation at different heights and directions which is configured to allow up to 65 atmospheric layers and 40 radiation streams (40 zenith angles and 40 azimuthal modes) [14].

2.4 Extraterrestrial Source Spectra

SBDART has three extraterrestrial solar spectrum models to be used. LOWTRAN-7 solar spectrum [20] employed in this study is based on measurements between 300 and 610 nm and uses a λ^{-4} power law for longer wavelengths.

The second alternative, MODTRAN-3 model is a composite of information gathered by several different spectral measurement campaigns that firstly wavelengths between 174 and 351 nm the spectral information is based on observations made with the Solar Ultraviolet Spectral Irradiance Monitor flown on Spacelab 2 [21], secondly wavelengths between 351 and 868 nm are based on the results of Neckel and Labs [22], thirdly the observations of Wehrli [23] are used for wavelengths between 0.868 and 3.226 μm and finally, for wavelengths greater 3.23 μm , the longwave power law dependence of LOWTRAN-7 is used [20].

As a third option, the solar models used in 5s [24] may be run with SBDART.

CHAPTER 3

RADIATIVE-CONVECTIVE MODEL, RADIATION MODEL AND NUMERICAL SOLUTION PROCEDURE

In this chapter, the code RCM4EAS, developed for estimation of the atmospheric and surface temperatures in the 1-D plane-parallel atmosphere and investigation of the sensitivity of earth-atmosphere system to the changes in the CO₂ concentration is described. Radiative-Convective Model (RCM) used in this study is described in the first section while detailed explanation of the theory and the working form of equations of the radiation model are given in the second section. In the last section, numerical solution procedure followed in RCM4EAS regarding the coupling procedure of the RCM and SBDART is represented.

3.1 RADIATIVE-CONVECTIVE MODEL

In this section, description of the energy budget of the earth-atmosphere system related to the radiative and convective processes taking place in this system was given in detail. In the first part of this section, general description of the model and the model input parameters are represented while in the second part estimation of radiative heating/cooling rates in the atmospheric layers and the ocean-layer using radiative fluxes is described. A brief description of the convective processes, namely the convective-adjustment procedure and estimation of the radiative-convective equilibrium temperatures are given in the third part of this section.

3.1.1 Description of the Model and Input Parameters

A 1-D RCM was developed in an attempt to estimate the vertical distribution of the temperatures within the earth-atmosphere system consisting of the atmosphere and the ocean layer. As can be seen in Figure 3.1, atmosphere is divided into homogeneous layers each having constant radiative properties and uniform temperature that may vary from layer to layer:

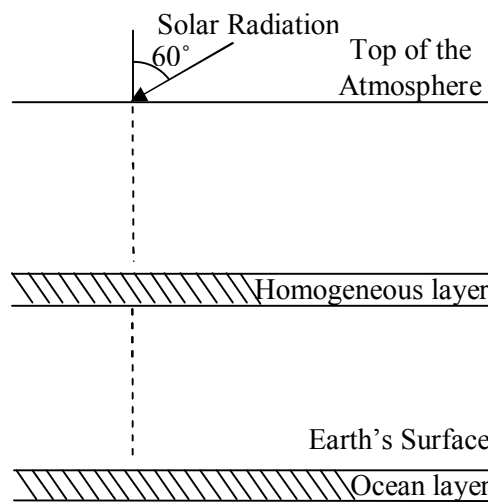


Figure 3.1 Schematic representation of plane-parallel atmosphere

Characterized by its top height, thickness, average droplet size and liquid water path, a cloud can be put into any layer.

The ocean layer has a certain thickness, Δh , and it was assumed that it only exchanges energy with the atmosphere not with the deeper ocean. An ocean layer thickness of 100 m was used unless otherwise stated.

The atmosphere was subjected to a known incident radiation from the sun with an average zenith angle of 60° and solar radiation was halved in order to account for an average daylight length of 12 hours.

Estimation of solar fluxes were carried out in short wavelength (SW) spectrum covering a range of 0.2 μm to 5 μm while infrared fluxes were calculated in long wavelength (LW) spectrum within the range of 4 μm to 100 μm . It was assumed that incident radiation from the top of the atmosphere is included in the short wave region only and the earth's surface has a certain value of reflectivity, 0.1, that the upward solar flux density at the ground is the product of the value of total downward solar radiation reaching the ground and the surface reflectivity. Black body ground emission was assumed in the infrared calculations. Details of the calculation of radiative fluxes are given in Section 3.2.

There are several absorbers in the atmosphere among which H_2O , O_3 , CO_2 , have relatively more importance in the climate studies. Remaining absorbers that are uniformly distributed over the atmosphere with specified (v/v) mixing ratios are given in Table 3.1:

Table 3.1 Various atmospheric absorbers and corresponding mixing ratios in ppm

N_2	O_2	CH_4	N_2O	CO	NH_3	SO_2	NO	HNO_3	NO_2
781.10^3	209.10^3	1.74	0.32	0.15	5.10^{-4}	3.10^{-4}	3.10^{-4}	5.10^{-5}	23.10^{-6}

In order to account for the variation of the water vapor, the relative humidity in the atmosphere was calculated following Manabe et al. [25]. Vertical distribution of relative humidity throughout the atmosphere was estimated with following relation:

$$R_i(T_i) = R_0 \frac{P_i/P_0 - 0.02}{1 - 0.02} \quad (3.1)$$

where P_i and R_i is the pressure and the relative humidity at the i^{th} atmospheric level respectively, R_0 is the surface relative humidity that was assumed to be 0.77 and P_0 is the surface pressure taken as 1 atm.

Once the vertical distribution of the relative humidity is known, partial pressure of the water vapor at each atmospheric level, $P_{H_2O,i}$, can be found using the definition of the relative humidity as:

$$P_{H_2O,i} = P_{H_2O}^{sat}(T_i)R_i(T_i) \quad (3.2)$$

where $P_i^{sat}(T_i)$ is the saturation pressure of water vapor at the i^{th} atmospheric level estimated by Clausius-Clapeyron equation as:

$$P_{H_2O}^{sat}(T_i) = P_{H_2O}^{sat}(273) \exp\left(\frac{M_{w,H_2O}}{M_{w,air}} \frac{L_i(T_i)}{R/M_{w,air}} \left(\frac{1}{273} - \frac{1}{T_i}\right)\right) \quad (3.3)$$

where R is the ideal gas constant, 8.314 kJ/kg/K and L_i is the latent heat of evaporation at the i^{th} atmospheric level, kJ/kg.H₂O, calculated according to the following relation [26]:

$$L_i(T_i) = 2510 - 2.38(T_i - 273) \quad (3.4)$$

Density of the water vapor at each atmospheric level was calculated using Eq. (3.2 to 3.4) and the ideal gas law as:

$$\rho_{H_2O,i} = P_{H_2O,i} / RT_i \quad (3.5)$$

CO₂ was assumed to be uniformly distributed in the atmosphere given an up-to-date mixing ratio (v/v) of 387 ppm [27] unless otherwise stated.

In the model, atmosphere was divided into 18 layers based on a sigma-pressure coordinate system adapted from Manabe et al. [5]. Mid-latitude summer atmospheric profile of McClatchey et al. [28], given in Figure 3.2 and 3.3 were used as initial temperature and O₃ concentration profiles in the model.

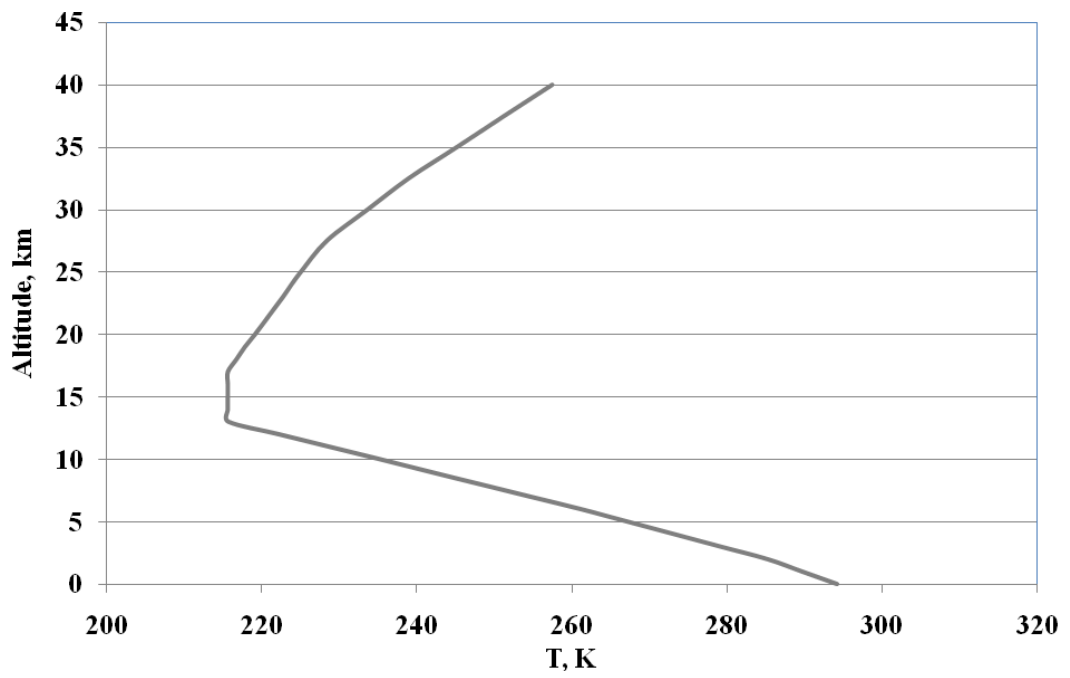


Figure 3.2 Model input Temperature profile [28]

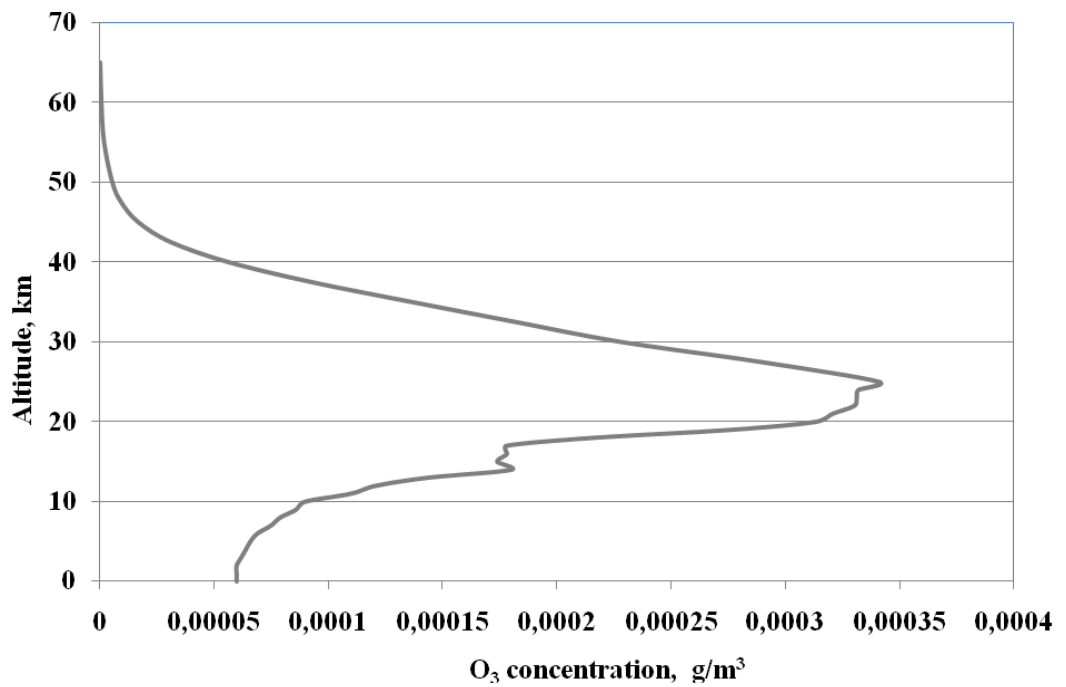


Figure 3.3 Model input O₃ concentration profile [28]

3.1.2 Estimation of Radiative Atmospheric Temperatures

Radiation processes accompanied with appropriate convective adjustment mechanisms play a major role in temperature changes on earth-atmosphere system.

Computed Solar and IR Fluxes within the atmosphere can be used to calculate the atmospheric and surface heating rates which in turn can be used to compute the temperature of atmospheric layers and the ocean layer.

A schematic representation of one dimensional plane parallel atmosphere model is given in Figure 3.4. Note that, terms associated with atmospheric levels such as upward and downward fluxes and pressure levels are denoted by subscript-i while layer-average terms such as temperatures and heating/cooling rates are denoted by subscript-j. Surface related parameters are denoted by subscript-1 as can be seen from the figure.

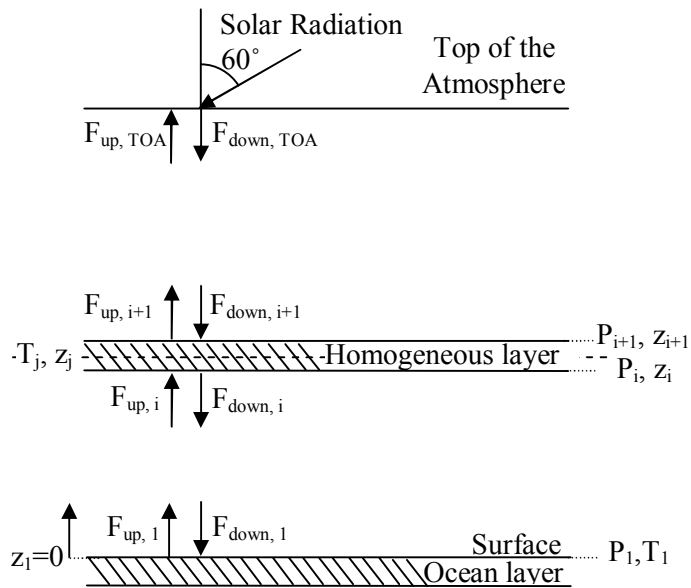


Figure 3.4 Schematic representation of fluxes used in the model

3.1.2.1 Solar Heating Rates in the Atmosphere

As a consequence of the absorption of the incoming solar radiation, the net flux density decreases from the top of the atmosphere to the surface. The absorbed solar radiation within an atmospheric layer can be related to the difference between the incoming solar flux at the upper level and the leaving solar flux at the lower level of that particular layer.

Net solar flux at each atmospheric level can be defined as in Eq. (3.6) so that a positive net flux is obtained:

$$(\text{Net Solar Flux})_i^S = (\text{Downward Solar Flux})_i^S - (\text{Upward Solar Flux})_i^S = F_{down,i}^S - F_{up,i}^S \quad (3.6)$$

Note that the atmospheric parameters related with solar radiation such as radiative fluxes and atmospheric heating rates are denoted with superscript-S.

Absorbed radiant energy results in heating of the atmospheric layer according to the energy conservation principle. Temperatures of the atmospheric layers can be estimated using the time rate of temperature changes within each layer, namely the heating rate of each layer. Once absorbed solar radiation of the specified layer is computed, heating rate of each atmospheric layer due to solar radiation can be obtained by Eq. (3.7).

$$\left(\frac{dT}{dt}\right)_j^S = \frac{1}{\rho C p_a} \left(\frac{dF}{dz}\right)_j^S \quad (3.7)$$

Expressing Eq. (3.7) in terms of pressure coordinates using the hydrostatic equation; Eq. (3.8) is obtained.

$$\left(\frac{dT}{dt}\right)_j^S = \frac{g}{C p_a} \left(\frac{dF}{dP}\right)_j^S = \frac{g}{C p_a} \frac{F_{net,i+1}^S - F_{net,i}^S}{P_i - P_{i+1}} \quad (3.8)$$

where $dP = \rho g dz$, from the hydrostatic equation [1] and $C p_a$ is the heat capacity of air.

3.1.2.2 Infrared Cooling Rates in the Atmosphere

The atmosphere loses radiative energy to space through thermal infrared (IR) emission therefore cooling rates (or negative heating rates) arise from IR emission in the atmosphere [1].

Similar to the definition of the solar heating rate, infrared cooling rate of each atmospheric layer can be defined as:

$$\left(\frac{dT}{dt}\right)_j^{IR} = \frac{g}{Cp_a} \left(\frac{dF}{dP}\right)_j^{IR} = \frac{g}{Cp_a} \frac{F_{net,i+1}^{IR} - F_{net,i}^{IR}}{P_i - P_{i+1}} \quad (3.9)$$

where the atmospheric parameters related with infrared radiation such as radiative fluxes and cooling rates are denoted with superscript-IR. Note that net IR flux at each atmospheric level is defined in an opposite manner so that a positive net flux is obtained given in Eq. (3.10).

$$(\text{Net IR Flux})_i^{IR} = (\text{Upward IR Flux})_i^{IR} - (\text{Downward IR Flux})_i^{IR} = F_{up,i}^{IR} - F_{down,i}^{IR} \quad (3.10)$$

3.1.2.3 Net Rate of Temperature Changes in the Atmosphere

Net rate of temperature change of each atmospheric layer due to radiative processes can be defined as the difference between the solar heating rate and the IR cooling rate as follows:

$$\left(\frac{dT}{dt}\right)_j^N = \left(\frac{dT}{dt}\right)_j^S - \left(\frac{dT}{dt}\right)_j^{IR} \quad (3.11)$$

Eq. (3.11) can be integrated using appropriate integration algorithms to obtain temperature of the layer within the specified time interval. In this study, this is done by time integration due to its simplicity as shown in Eq. (3.12) [7]:

$$\Delta T = \Delta t \left(\frac{dT}{dt} \right)_j^N \quad (3.12)$$

Temperature change estimated in the described manner is used to compute the temperature of the atmospheric layers within the present time step and this procedure is continued until the temperature of each layer is reasonably close to that of the previous time step.

3.1.2.4 Heating Rate in the Ocean Layer

In order to define the rate of change of ocean layer (or the surface) temperature, balance of radiative and convective fluxes should be constructed at the surface. The energy budget of the ocean layer involves net downward solar radiation and downward IR radiation to the surface, the upward IR radiation emitted from the surface as a result of the heating due to the net downward radiation and the convective flux that accounts for the effect of the transport of sensible and latent heat fluxes out of the surface (c.f. section 3.1.3) as shown in Eq. (3.13):

$$\left(\frac{dT}{dt} \right)_1 = \frac{1}{\rho_w C_p \Delta h} \left(F_{down,1}^S + F_{down,1}^{IR} - F_{up,1}^{IR} - F^{CN} \right) \quad (3.13)$$

where Δh is the depth of the ocean layer, C_p is the heat capacity of water and ρ_w is the density of water.

Eq. (3.13) can be integrated to give temperature of the ocean layer within the present time step similar to the estimation of atmospheric temperatures described in section 3.1.2.3.

Temperature of the ocean layer computed in this manner is then equated to the earth's surface temperature that is one of the major assumptions of the model developed in this study.

3.1.3. Convective Adjustment

Convective adjustment is based on the concept of static stability [1] which is referred as the ability of a fluid at rest to become turbulent or laminar due to the effects of buoyancy. The instability caused by some outside forcing such as the temperature difference between two adjacent atmospheric layers, will be reduced or eliminated with the help of turbulence formed in statically unstable air by moving the less dense fluid up and the more dense fluid down, and creating a neutrally buoyant mixture [29].

In the convective adjustment procedure, the effects of convection are included implicitly by assuming that convection maintains a critical temperature lapse rate, i.e. the rate of temperature decrease with height in the atmosphere at which the atmosphere is in a neutral state, within the convective region [6]. In order to do this, temperatures of the adjacent atmospheric layers are adjusted whenever the critical lapse rate is exceeded so that more realistic temperatures are attained in the atmosphere [5]. Since the lapse rate of climatological atmospheric temperature profile in the troposphere is nearly 6.5 K/km, this value is used in conventional convective adjustment procedure approach [1].

After the temperatures of atmospheric layers and the ocean layer are computed using radiative heating/cooling rates, the lapse rate, general expression of which is given in Eq. (3.14), between the ocean layer and the first layer is estimated and if the lapse rate is below the critical lapse rate then temperatures are not adjusted [7].

$$(LAP)_j = \frac{T_j - T_{j+1}}{z_{j+1} - z_j} \quad (3.14)$$

Provided that the lapse rate exceeds the predetermined critical lapse rate, convective adjustment is carried out by transferring heat energy from the ocean layer to the first atmospheric layer in compliance with the energy conservation principle. Adjusted temperatures of the first atmospheric layer (T_2^{adj}) and the ocean layer (T_2^{adj}) providing the critical lapse rate condition are computed using the energy

conservation equation and opposed critical lapse rate condition given in Eq. (3.15) and Eq. (3.16), respectively.

$$\rho_w \Delta h C p_w (T_1^{pre} - T_1^{adj}) + \frac{\Delta P_2}{g} C p_a (T_2^{adj} - T_2^{pre}) = 0 \quad (3.15)$$

$$T_1^{adj} - T_2^{adj} - CLR(z_2 - z_1) = 0 \quad (3.16)$$

After the convective adjustment procedure described above is carried out, lapse rate between the first and the second atmospheric layers is estimated using the newly computed (or unchanged) temperature of the first atmospheric layer (T_2^{adj}) and the present temperature of the second atmospheric layer (T_3^{pre}). Again if the computed lapse rate is below the critical lapse rate, temperatures of the atmospheric layers are kept unchanged, if the opposite is true then the convective adjustment procedure described previously is performed and modified atmospheric temperatures satisfying the critical lapse rate condition are obtained using Eq. (3.17) and Eq. (3.18) given below:

$$\frac{\Delta P_2}{g} C p_a (T_2^{pre} - T_2^{adj}) + \frac{\Delta P_3}{g} C p_a (T_3^{adj} - T_3^{pre}) = 0 \quad (3.17)$$

$$T_2^{adj} - T_3^{adj} - CLR(z_3 - z_2) = 0 \quad (3.18)$$

Above mentioned process is proceeded going upwards for all atmospheric layers [7]. After going through the surface and all atmospheric layers, this procedure is repeated till the newly computed (or unchanged) temperature of the surface and the atmospheric layers come out to be in accordance with the pre-determined critical lapse rate.

Finally, the change in the net content of energy of the atmospheric layers is removed from the surface in order to balance the energy account due to the convective adjustment procedure by using Eq. (3.19) [7]:

$$\rho_w \Delta h C_{p_w} (T_1^{adj} - T_1^{pre}) = \sum_{i=2}^{nt} \frac{\Delta P_i}{g} C_{p_a} (T_i^{adj} - T_i^{ini}) \quad (3.19)$$

where T_i^{ini} is the temperature of the i^{th} atmospheric layer prior to the adjustment procedure and nt is the highest atmospheric layer undergoing temperature change due to convective adjustment.

Eq. (3.19) can be manipulated to give the convective flux as can be seen in Eq. (3.20), F^{CN} , which can be used to demonstrate the effect of the transport of sensible and latent heat fluxes out of the surface in Eq. (3.13).

$$F^{CN} = \frac{1}{\Delta t} \sum_{i=2}^{nt} \frac{\Delta P_i}{g} C_{p_a} (T_i^{adj} - T_i^{ini}) \quad (3.20)$$

3.2 RADIATION MODEL

In this section, radiation model based on discrete ordinate method (DOM) is described for modeling of radiative transfer in plane parallel atmosphere. Radiative transfer equation (RTE) and boundary conditions (BCs) pertaining to the RTE are briefly described in the first part whilst the numerical solution procedure followed for discretization of RTE utilizing DOM is given in the second part. This is followed with the description of the radiative property estimation technique, exponential sum-fitting method, employed in this study.

3.2.1 The Radiative Transfer Equation (RTE)

The differential change of diffuse intensity emergent from below within a layer of thickness Δz is due to the following processes: (1) attenuation by extinction, (2) single scattering of the unscattered solar flux, (3) multiple scattering and (4) emission from the layer as illustrated in Figure 3.5.

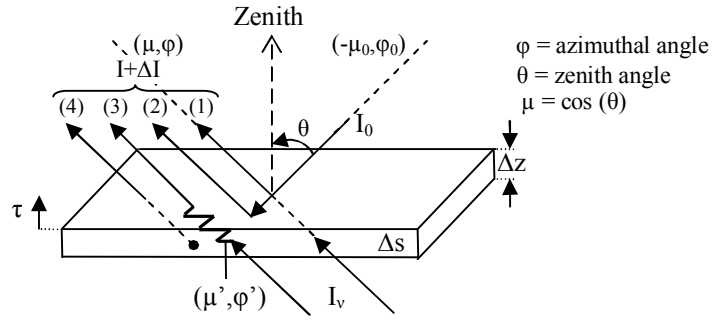


Figure 3.5 Transfer of intensity from below in plane-parallel layers [1]

Considering a small volume containing a spectrum of molecules and/or particulates and noting that the differential length is $\Delta s = \Delta z / \mu$, monochromatic radiative transfer equation (RTE) in plane parallel atmospheres can be given in Eq. (3.21):

$$\frac{\Delta I_v(z; \mu, \varphi)}{\Delta z / \mu} = -\beta_{e,v} I_v(z; \mu, \varphi) + \beta_{s,v} \int_0^1 \int_{-1}^1 I_v(z; \mu', \varphi') P_v(\mu, \varphi; -\mu', \varphi') / 4\pi d\mu' d\varphi' \quad (3.21)$$

$$+ \beta_{s,v} I_0 e^{-\tau/\mu} P_v(\mu, \varphi; -\mu_0, \varphi_0) / 4\pi + \beta_{a,v} B_v[T(z)]$$

where $P(\mu, \varphi; \mu', \varphi')$ is the phase function representing the redirection of the incoming intensity (μ, φ) to the outgoing intensity (μ', φ') and β_e , β_s and β_a are the extinction, scattering, and absorption coefficients (in units of per length) respectively given by:

$$\beta_{e,s,a} = \int_{\Delta z} \sigma_{e,s,a}(z) n(z) dz / \Delta z \quad (3.22)$$

where σ is the cross section and n is the number density.

In Eq. (3.21), the first term is associated with attenuation of the incoming intensity while the remaining terms represent augmentation due to multiple scattering, single scattering and emission, respectively.

Furthermore introducing the single scattering albedo, $\omega = \beta_s / \beta_e$ (or $1 - \omega = \beta_a / \beta_e$) and the optical depth, $\tau = \int_z^\infty \beta_e dz'$ to Eq. (3.21) gives monochromatic RTE at frequency ν as an Eq. (3.23).

$$\begin{aligned} \mu \frac{dI_\nu(\tau; \mu, \varphi)}{d\tau} = & I_\nu(\tau; \mu, \varphi) - \frac{\omega_\nu}{4\pi} \int_0^1 \int_{-1}^1 I_\nu(\tau; \mu', \varphi') P_\nu(\mu, \varphi; \mu', \varphi') d\mu' d\varphi' \\ & - \frac{\omega_\nu}{4\pi} I_0 P_\nu(\mu, \varphi; -\mu_0, \varphi_0) e^{-\tau/\mu_0} - (1 - \omega_\nu) B_\nu[T(\tau)] \end{aligned} \quad (3.23)$$

where $I_\nu(\tau, \mu, \varphi)$ is the spectral radiative intensity at position τ in the direction $\Omega(\mu, \varphi)$, φ and θ are the azimuthal and zenith angles respectively and μ is the direction cosine or equivalently the cosine of zenith angle, $\cos(\theta)$, as shown in Figure 3.6.

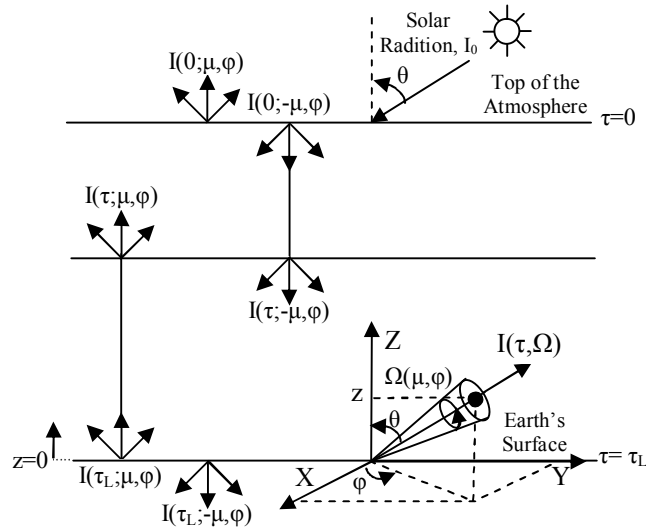


Figure 3.6 Schematic drawing and geometry of plane-parallel atmosphere [1]

As can be seen from Figure 3.6 the upward intensity is indicated with a (+) sign while the downward intensity is indicated with a (-) sign prior to μ .

Eq. (3.23) can be reduced to a more compact form that is required for the foregoing discussions as in Eq. (3.24).

$$\mu \frac{dI_v(\tau_v; \mu, \varphi)}{d\tau} = I_v(\tau_v; \mu, \varphi) - \frac{\omega_v(\tau_v)}{4\pi} \int_0^{2\pi} \int_{-1}^1 I_v(\tau; \mu', \varphi') P_v(\mu, \varphi, \mu', \varphi') d\mu' d\varphi' - Q_v(\tau_v; \mu, \varphi) \quad (3.24)$$

where $Q_v(\tau; \mu, \varphi)$ is the source term given in Eq. (3.25) stemming from (1) a parallel beam incident in direction μ_0, φ_0 , i.e., $Q_v^b(\tau; \mu, \varphi)$ and (2) thermal emission in local thermodynamic equilibrium, i.e., $Q_v^t(\tau)$:

$$\begin{aligned} Q_v(\tau_v; \mu, \varphi) &= Q_v^b(\tau_v; \mu, \varphi) + Q_v^t(\tau_v) \\ &= \frac{\omega_v(\tau_v)}{4\pi} I_0 P_v(\tau_v, \mu, \varphi; -\mu_0, \varphi_0) e^{-\tau_v/\mu_0} + (1 - \omega_v(\tau_v)) B_v [T(\tau_v)] \end{aligned} \quad (3.25)$$

where $B_v[T(\tau_v)]$ is defined as the Plank function at frequency ν .

Eq. (3.24) is subjected to the following boundary conditions (BC's):

Top BC: atmosphere is subjected to known incident beam intensity, I_0 ,

$$I_v(\tau_v = 0; -\mu, \varphi) = I_{0,v}(-\mu) \quad (3.26)$$

Bottom BC: upward intensity leaving the earth's surface is defined as:

$$\begin{aligned} I_v(\tau_L, +\mu, \varphi) &= \varepsilon_v(\mu) B_v [T(\tau_{g,v})] + \frac{1}{\pi} \int_0^{2\pi} d\varphi' \int_0^1 \rho_{d,v}(\mu, \varphi; -\mu', \varphi') I_v(\tau_{L,v}; -\mu', \varphi') \mu' d\mu' \\ &\quad + \frac{\mu_0}{\pi} I_0 e^{-\tau_L/\mu_0} \rho_{d,v}(\mu, \varphi; -\mu_0, \varphi_0) \end{aligned} \quad (3.27)$$

where T_g is surface temperature and $\rho_d(\mu, \varphi, -\mu_0, \varphi_0)$ is bidirectional reflectivity [19].

Applying the Kirchhoff's law ($\alpha_v = \varepsilon_v$) and assuming that the transmissivity of the earth's surface is negligible, the directional emissivity, $\varepsilon(\mu)$, can be defined as:

$$\varepsilon_v(\mu) = 1 - \frac{1}{\pi} \int_0^{2\pi} d\varphi' \int_0^1 \rho_{d,v}(\mu, \varphi; -\mu', \varphi') \mu' d\mu' \quad (3.28)$$

In order to simplify the notation, subscript- v is omitted in the foregoing discussions; consequently Eq. (3.24) takes the following form:

$$\mu \frac{dI(\tau; \mu, \varphi)}{d\tau} = I(\tau; \mu, \varphi) - \frac{\omega(\tau)}{4\pi} \int_0^1 \int_{-1}^1 I(\tau; \mu', \varphi') P(\mu, \varphi; \mu', \varphi') d\mu' d\varphi' - Q(\tau; \mu, \varphi) \quad (3.29)$$

Legendre polynomials can be used to numerically expand the phase function, $P(\mu, \varphi; \mu', \varphi')$, with a finite number of terms. The intensity, $I(\tau; \mu, \varphi)$, and the source term, $Q(\tau; \mu, \varphi)$, can also be expanded similar to the phase function expansion. Once the phase function is expanded in a series of $2N$ Legendre polynomials with the intensity and the source term is expanded in a Fourier cosine series, Eq. (3.29) turns into $2N$ independent equations (one for each Fourier component) as:

$$\mu \frac{dI^m(\tau, \mu)}{d\tau} = I^m(\tau, \mu) - \int_{-1}^1 D^m(\tau, \mu, \mu') I^m(\tau, \mu') d\mu' - Q^m(\tau, \mu) \quad (3.30)$$

$m = 0, \dots, 2N-1$

A more detailed discussion of utilization of Legendre polynomials in the radiative transfer calculations and derivation of Eq. (3.30) are given in Appendix A.

3.2.2 Discrete Ordinates Method (DOM)

The discrete-ordinates method, developed by Chandrasekhar [30] for application to the transfer of radiation in planetary atmospheres, has been found to be an efficient and accurate method for calculation of scattered intensities and fluxes that involves the discretization of the basic radiative transfer equation and the solution of a set of first-order differential equations [1]. Originally designed to describe radiative transfer in homogeneous media, DOM has been extended for use in inhomogeneous atmospheres consisting of adjacent homogeneous layers in which the scattering and the absorption properties may vary in different layers [31].

Reduction of the resulting integro-differential equation, Eq. (3.30), to the systems of ordinary differential equations is the essence of DOM which is done by replacing the integral by a summation over a finite number of quadrature points. For quadratures in the interval (-1,1), Gauss's formula has been found to be superior to other formulas in which integral of any function $f(\mu)$ may be represented as in Eq. (3.31):

$$\int_{-1}^1 f(\mu) d\mu \approx \sum_{j=-N}^N w_j f(\mu_j) \quad (3.31)$$

where w_j are the quadrature weights associated with the directions μ_j (quadrature points) and N is the number of discrete directions.

The discrete ordinate approximation of Eq. (3.30) can be given as:

$$\mu_i \frac{dI^m(\tau, \mu_i)}{d\tau} = I^m(\tau, \mu_i) - \sum_{\substack{j=-N \\ j \neq 0}}^N w_j D^m(\tau, \mu_i, \mu_j) I^m(\tau, \mu_j) - Q^m(\tau, \mu_i) \quad (3.32)$$

$i = \pm 1, \dots, \pm N$

A detailed discussion of the numerical solution of the discretized form of RTE, Eq. (3.32), for each pre-divided atmospheric layer is given in Appendix B.

Constituting of (for each m) a system of $2N$ coupled differential equations with non-constant coefficients, single scattering albedo, $\omega(\tau)$, and the phase function, $P(\tau, \cos\theta)$, Eq. (3.32) can not be solved analytically. In order to obtain analytical solutions, it is assumed that the thermal source term, $Q_v^{\dagger}(\tau)$, can be expressed by a polynomial as function of τ and the inhomogeneous atmosphere consists of L adjacent homogeneous layers with constant scattering and absorption properties that vary in different layers as can be seen in Figure 3.7. Note that physical constants associated with homogeneous layers are denoted by subscript- p .

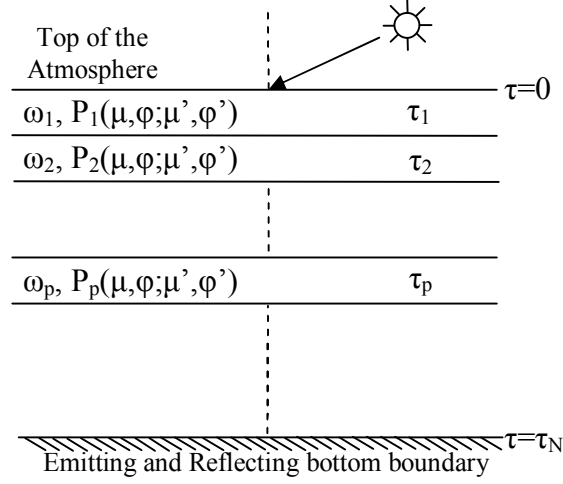


Figure 3.7 Schematic representation of the multilayered medium [19]

The general form of the discrete ordinate solution to Eq. (3.32) including BC's should be given in the following form [19]:

$$I_p(\tau, \mu_i) = \sum_{j=1}^N [C_{jp} G_{jp}(\mu_i) e^{-k_{jp}\tau} + C_{-jp} G_{-jp}(\mu_i) e^{k_{jp}\tau}] + R_p(\tau, \mu_i) \quad (3.33)$$

$$k_{jp} > 0 \text{ and } k_{-jp} = -k_{jp}$$

where k_{jp} and G_{jp} are previously obtained eigenvalues and eigenvectors of each layer respectively while $R_p(\tau; \mu_i)$ is the particular solution given as:

$$R_p(\tau, \mu_i) = Z_0(\mu_i) e^{-\tau/\mu_0} + \delta_{m0} [Y_0(\mu_i) + Y_1\tau] \quad (3.34)$$

Eq. (3.33) constitutes a system of $(2N \times L) \times (2N \times L)$ linear algebraic equations to be solved in order to obtain $(2N \times L)$ unknown coefficients, C_{jp} , ($j = \pm 1, \dots, \pm N$; $p = 1, \dots, L$) as described in Appendix B in detail.

3.2.2.1 Angular Quadrature Scheme of DOM

The angular quadrature scheme and order of approximation used to estimate quadrature points (μ_j) and weights (w_j) in Eq. (3.32) plays an important role for the predictive accuracy of DOM. Unlike the quadrature rule adopted by Chandrasekhar [30] that applies Gaussian formula for the complete range $-1 < \mu < 1$, double-gauss scheme is used in this study in which the Gaussian formula is applied separately to the half ranges; $-1 < \mu < 0$ and $0 < \mu < 1$.

Double Gauss scheme provides superior results near the boundaries where the intensity varies rapidly around $\mu_j=0$ and in the boundaries where intensity discontinuities are encountered [19].

The abscissa for ordinary Gaussian quadrature on the interval (0,1) are computed as roots of the Legendre polynomial $P_n(\mu_j)$ using a cubically convergent refinement of Newton's method [32].

This is done by following an iterative procedure where μ_j 's associated with the order of the approximation, N, are calculated using Eq. (3.35):

$$\mu_j^{t+1} = \mu_j^t - \frac{P_n(\mu_j)}{P_n'(\mu_j)} \left(1 + \frac{P_n(\mu_j)}{P_n'(\mu_j)} \frac{P_n''(\mu_j)}{2P_n'(\mu_j)} \right) \quad (3.35)$$

where μ_j^{t+1} is the quadrature point to be estimated using the previous estimate, μ_j^t .

The following equation can be used to obtain the initial guess required in Eq. (3.35):

$$\mu_j^t = \frac{4n-1}{4j+1} \pi + \frac{n-1}{8n^3} \cot \left(\frac{4n-1}{4j+1} \pi \right) \quad (3.36)$$

Given the initials values of $P_{n-1}(\mu_j)$ ($=\mu_j$) and $P_{n-2}(\mu_j)$ ($=1$), Legendre polynomials used in Eq. (3.35) can be calculated according to the recurrence relation [32]:

$$nP_n(\mu_j) = (2n-1)\mu_j P_{n-1}(\mu_j) - (n-1)P_{n-2}(\mu_j) \quad (3.37)$$

$n \geq 2$

The derivatives in Eq. (3.35) can be computed through the orthogonal polynomials itself [32]:

$$(1 - \mu_j^2)P_n'(\mu_j) = n(P_{n-1}(\mu_j) - \mu_j P_n(\mu_j)) \quad (3.38)$$

The corresponding quadrature weights, w_j , can then be calculated by:

$$w_j = \frac{2(1 - \mu_j^2)}{(nP_{n-1}(\mu_j))^2} \quad (3.39)$$

In Table 3.2, parameters associated with the choice of the order of approximation regarding the direction cosines and weights for one-dimensional parallel plane atmosphere are tabulated.

Table 3.2 Direction cosines and weights specified by order of approximation

Order of Approximation (=N)	# of streams (=2N)	Ordinates μ_j	Weights w_j
2	4	0.21132487	0.50000000
		0.78867513	0.50000000
4	8	0.06943184	0.17392742
		0.33000948	0.32607258
		0.66999052	0.32607258
		0.93056816	0.17392742
8	16	0.01985507	0.05061427
		0.10166676	0.11119052
		0.23723380	0.15685332
		0.40828268	0.18134189
		0.59171732	0.18134189
		0.76276621	0.15685332
		0.89833324	0.11119052
		0.98014493	0.05061427

3.2.3 Radiative Property Estimation Technique: Exponential-Sum Fitting

Exact calculations of the absorption spectrum are carried out by the line-by-line models which necessitate determination of absorption coefficient along the shape of each individual spectral line so that they require much of a computational effort and are usually performed for benchmarking purposes only. In the atmosphere, these calculations have to be performed for many altitudes since gaseous concentrations, half-widths and line intensities depend on pressure and temperature which makes them computationally much more expensive.

The need for less costly yet sufficiently reliable solutions to RTE leads to the development of computationally more efficient radiative property estimation methods. Band models are among the very first of these methods that are basically characterized with making use of the averages over many lines. Alternatively, the average transmission of a particular gas in a particular wave number band can be described by using certain parameterization techniques which is more advantageous being considerably faster than the band model approach [33]. The *exponential sum-fitting* is one of the most successful representatives of this method which is the radiative property estimation technique employed in SBDART.

Exponential sum-fitting is an approximation of the transmission function for a given interval $\Delta\nu$ by an exponential expression in the following form:

$$T_{\Delta\nu}(u) = \frac{1}{\Delta\nu} \int_{\Delta\nu} \exp(-k_\nu u) d\nu \approx \sum_{i=1}^m a_i \exp(-b_i u) \quad (3.40)$$

where k_ν is the absorption coefficient, u is the optical mass and $\Delta\nu$ is the spectral interval in which the transmittance is defined.

The goal is to find the coefficients defined in Eq. (3.40) that are the dimensionless positive weight, a_i , and the corresponding gray absorption coefficient, b_i , so that the mean transmission over the spectral interval $\Delta\nu$ can be expressed as the sum of m partial transmissions meeting the constraints given in Eq. (3.41) and Eq. (3.42).

$$\sum_{i=1}^m a_i = 1, a_i > 1, b_i \geq 0 \quad \text{for all } i \quad (3.41)$$

The least-squares technique was successfully adopted for estimation of reliable coefficient pairs (a_i, b_i) [33] considering that $T_{\Delta v}$ can be approximated with:

$$E_{\Delta v}(u_n) = \sum_{i=1}^m a_i \exp(-b_i n \Delta u) = \sum_{i=1}^m a_i \theta^n \quad (3.42)$$

where u_n is the arbitrary absorber mass defined in the grid consisting of uniform absorber mass increments, Δu , so that $u_n = n \Delta u$.

The difference between the approximated mean transmission, $E_{\Delta v}(u_n)$, and its exact value, $T_{\Delta v}(u_n)$, for equally spaced arguments can be expressed by the least squares residual as:

$$R_0 = \sum_{i=1}^N w_n [T_{\Delta v}(u_n) - E_{\Delta v}(u_n)]^2 \quad (3.43)$$

where w_n are the least square weights.

Among all the possibilities corresponding to different values of the parameters, a_i , b_i , and m ; the best fit is the one that minimizes the value of R_0 . Considering that the value of θ_i is known, the standard linear least squares normal equations for a_1, \dots, a_m are given in Eq. (3.44 to 46):

$$P(\theta_i) = \frac{\partial R_0}{\partial a_i} = 0 \quad i = 1, \dots, m \quad (3.44)$$

where the residual polynomial, $P(\theta)$, can be defined as in Eq. (3.45).

$$P(\theta) = 2 \sum_{n=1}^N p_n \theta^n \quad n = 1, \dots, N \quad (3.45)$$

p_n are weighted point by point differences between $E_{\Delta v}(u_n)$ and $T_{\Delta v}(u_n)$, in Eq. (3.46).

$$p_n = w_n [E_{\Delta v}(u_n) - T_{\Delta v}(u_n)] \quad n = 1, \dots, N \quad (3.46)$$

A good approximation to the transmission function can be obtained by iterating back and forth between solving Eq. (3.47) for the coefficients a_i and improving toward Eq. (3.48) by adding a new exponential factor θ_i [18].

$$P(\theta_i) = 0 \quad n = 1, \dots, m \quad (3.47)$$

$$P(\theta) \geq 0, \quad 0 \leq \theta \leq 1 \quad (3.48)$$

3.3 NUMERICAL SOLUTION PROCEDURE

The code RCM4EAS, developed in this study involves basically two phases of computation that either of which acts as the feedback of the other: (1) calculation of the radiative-convective temperature profile using radiative fluxes in the atmosphere and (2) computation of the radiative fluxes by using atmospheric profiles of pressure, temperature and the concentration of atmospheric absorbers. This requires a firmly established coupling procedure in between for the estimation of a reliable thermal equilibrium temperature profile in the earth-atmosphere system. In this section, numerical solution procedure followed for coupling of the representatives of each computational phase: the radiative-convective model and the radiation model are described in detail.

As illustrated in Figure 3.8, coupling procedure involves estimation of the temperatures of the pre-specified atmospheric layers and the ocean layer by using the radiative fluxes that is followed by the estimation of the vertical distribution of the water vapor at that layers for newly computed atmospheric temperature profile and giving these data as input to the radiation model, SBDART, to be used for computation of radiative fluxes at each atmospheric level and at the surface in return.

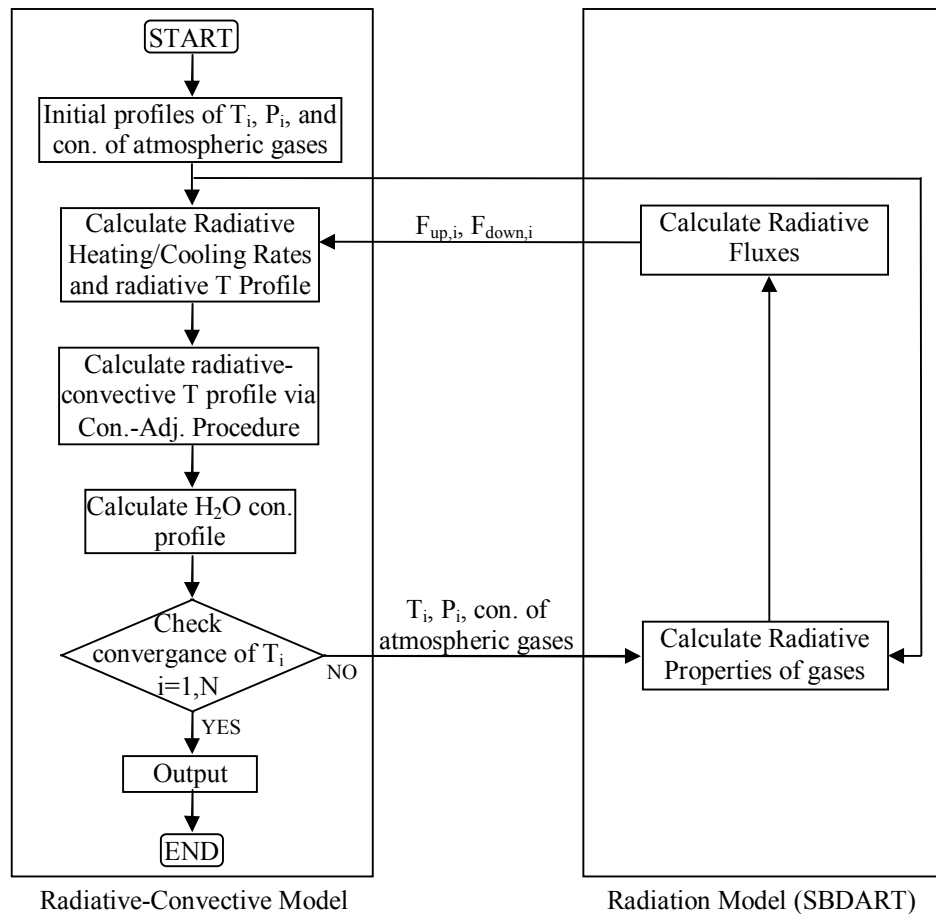


Figure 3.8 Flowchart of the coupled code, RCM4EAS

3.3.1 Algorithm of the code RCM4EAS

The algorithm of the coupled code, RCM4EAS, developed in this study, is given as:

1. Read in input data related with the Radiative-Convective Model (RCM) that includes number of atmospheric levels, time increment, ocean layer thickness, critical lapse rate and relative humidity at the surface.
2. Read in input data specifying the physics of the problem: the altitude, pressure and temperature of pre-determined atmospheric levels and layers.
3. Read in input data associated with the Radiation Model, SBDART, which are number of streams, wavelength increment and concentration of the atmospheric absorbers other than H₂O and O₃.
4. Read in input data specifying the physical properties of each cloud layer in the model atmosphere, if any, including liquid water path, effective particle diameter and cloud cover.
5. Set initial time of the computation.
6. Increase the time by an amount of time increment.
7. Set the previous values of the temperatures of each atmospheric layer and the surface to their present values.
8. Estimate the temperature of each atmospheric level using computational layer temperatures.
9. Estimate the H₂O concentration corresponding to each atmospheric level by using Eq. (3.1 to 3.5) via *subroutine* PH2O.
10. Estimate the O₃ concentration corresponding to each atmospheric level by using Mid-latitude summer vertical distribution of O₃.
11. Specify the atmospheric profiles of temperature, concentration of H₂O and O₃ and altitude of each computational level to be used as input in SBDART.

Calculation of Radiative Fluxes Using SBDART

12. Specify parameters to be used in SBDART such as the wavelength range, cosine of the solar zenith angle and surface reflectivity for calculation of Solar Fluxes.
13. Specify the position of each cloud layer in the model atmosphere, if any.
14. Set the initial wavelength of the computation.
15. Increase the wavelength by an amount of wavelength increment.
16. Calculate the optical depth due to atmospheric absorbers by using a three-term exponential fit for estimation of the mean transmissivity in the specified wavelength interval.
17. Calculate cloud optical depth and scattering parameters.
18. Calculate upward and downward spectral radiative fluxes corresponding to each computational level for each k-distribution term by using subroutine DISORT in the specified wavelength interval.
19. Check if the whole wavelength range is covered, go to step 15 otherwise.
20. Calculate the upward and downward radiative fluxes at each level integrated over the wavelength interval.
21. Repeat steps 12-20 for estimation of Infrared fluxes.

Calculation of Radiative Temperature Profile in the Atmosphere

22. Calculate net solar fluxes by differencing the downward solar flux from the upward solar flux at each atmospheric level.
23. Calculate net IR fluxes by differencing the upward IR flux from the downward IR flux at each atmospheric level.
24. Calculate the solar heating rate and IR cooling rate by using Eq. (3.8) and Eq. (3.9) respectively.

25. Calculate the net heating/cooling rate of each atmospheric layer by differencing the solar heating rate and IR cooling rate defined at each atmospheric layer.
26. Calculate the atmospheric radiation temperatures by integrating the time derivatives of each atmospheric layer found in step 25.

Calculation of the Temperature of the Ocean Layer

27. Calculate the net energy change in the atmosphere by summing up the energy increase/decrease of each layer due to convective adjustment procedure in the previous time step.
28. Calculate the temperature of the ocean layer by using Eq. (3.13).

Calculation of Radiative-Convective Temperatures

29. Adjust the altitude of each atmospheric layer and level using the newly computed temperatures in the atmosphere and the ocean layer by using *subroutine* ALTADJ.
30. Check the lapse rate between the ocean layer and the atmospheric layer adjacent to the ocean layer using Eq. (3.14) and perform convective adjustment procedure if the pre-determined critical lapse rate is exceeded using Eq. (3.15-16).
31. Check the lapse rate between the adjacent atmospheric layers and perform convective adjustment procedure if the pre-determined critical lapse rate is exceeded using Eq. (3.17-18) going from the lowest atmospheric layer to the uppermost atmospheric layer.
32. Repeat step 30-31 until critical lapse rate condition between all atmospheric layers is satisfied.
33. Calculate the net energy change in all atmospheric layers due to the convective-adjustment procedure using Eq. (3.20).

34. Calculate the absolute percent relative error between the newly calculated and previous estimate of the radiative-convective temperature at each atmospheric layer.
35. Check if the absolute percent relative error calculated for each computational layer is smaller than the pre-determined tolerance and go to step 7 if the convergence is not satisfied for each computational layer.
36. End RCM4EAS.

CHAPTER 4

RESULTS AND DISCUSSION

In this study, a 1-D radiative-convective model for earth-atmosphere system (RCM4EAS) was developed for both clear and cloudy sky conditions. The code uses a radiation code based on discrete ordinate method (DOM), namely Santa Barbara DISORT (Discrete Ordinate Radiative Transfer) Atmospheric Radiative Transfer (SBDART). The code was run with mid-latitude summer (MLS) data which consist of pressure, temperature and concentration profiles of radiatively active species within atmosphere up to 100 km. Sequence of code development is as follows. First the predictive accuracy of SBDART was tested by comparing its predictions with those of the most accurate method, Line-by-Line Radiative Transfer Model (LBLRTM). Sensitivity of the results of SBDART to spectral wavelength increment and number of streams was investigated. Optimum values of these parameters satisfying accuracy and computational efficiency were obtained for both clear and cloudy atmospheres. This was followed by the implementation of the coupled code to the investigation of the effect of doubling CO₂ concentration from today's value of 387 ppm for both clear and cloudy atmospheres. For the cloudy atmosphere application, typical cloud parameters for which predictions of radiative-convective model were available in literature were selected. Predicted surface equilibrium temperatures were compared with those of Hu et al. [11]. Finally, the effects of presence of cloud and doubling of the CO₂ concentration on equilibrium temperature profiles were investigated.

4.1 Benchmarking SBDART against LBLRTM

The accuracy of SBDART for clear sky was tested by benchmarking the computed net fluxes at specified altitudes with those of the LBLRTM code developed by Clough et al. [34] which is the analytical solution to the problem. Net fluxes were calculated for the long wavelength (LW) range 3.33-100 μm . The upper boundary of the wavelength was set to 100 μm as it is the highest allowable wavelength for computation of fluxes in SBDART.

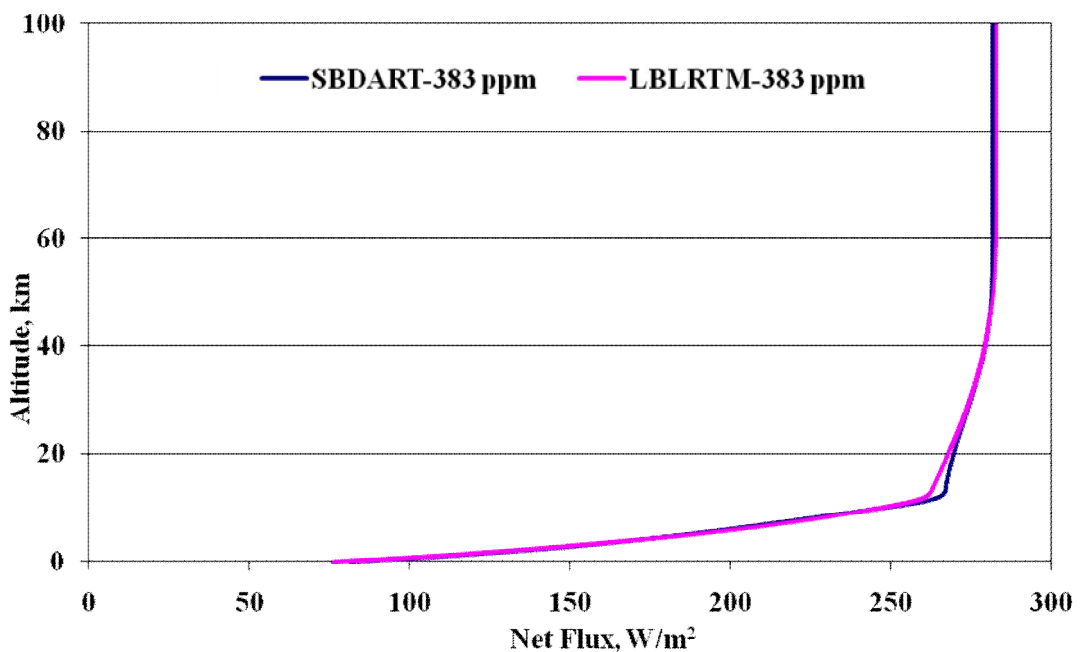


Figure 4.1 Comparison of net fluxes obtained by using LBLRTM and SBDART throughout the atmosphere

Figure 4.1 shows comparison between the net fluxes predicted by SBDART and LBLRTM. Good agreement is indicative of the fact that SBDART is an accurate method for computation of radiative fluxes throughout the atmosphere for LW range.

4.2 Effect of Wavelength Increment on Computational Efficiency and Accuracy of SBDART

Accuracy and efficiency of SBDART with regard to wavelength increment was tested by running the code for clear sky atmosphere on a personal computer with Pentium 4 2.80 GHz processor having 1.5 GB of RAM. Calculations were carried out for both short wavelength (SW) range (0.2-4.0 μm) and LW range (4.0-100 μm) in atmosphere up to 62 km adapted from Manabe et al. [5].

In order to determine the optimum wavelength increment in terms of computational efficiency and accuracy, SBDART was tested for various wavelength increments ranging from 0.001 to 1.0 and variable wavelength increment for computation of net fluxes in the atmosphere.

Variable wavelength ($\text{vwl}=0.01$) employs the wavelength increment as the constant fraction (0.01) of the current wavelength so that under-resolution of the short wavelength range and the over-resolution of the long wavelength range is avoided. The effect of wavelength performance on net fluxes was evaluated by comparing the predictions obtained from wavelengths in the range 0.01-1.00 μm with those estimated using a small wavelength increment (0.001 μm) for both clear and cloudy-sky atmosphere.

Table 4.1 shows the effect of wavelength increment (wl) on net fluxes for clear sky atmosphere. Average absolute percent relative error (APRE) is defined as:

$$APRE, \% = 100 \times \left| \frac{(\text{Net Flux at any } \text{wl}) - (\text{Net Flux at } \text{vwl} = 0.001)}{\text{Net Flux at } \text{vwl} = 0.001} \right| \quad (4.1)$$

Table 4.1 Effect of wavelength increment (wl) on net fluxes for clear sky

	wl=0.01		wl=0.1		wl=0.25		wl=0.5		wl=1.0		vwl=0.01	
	SW	LW	SW	LW	SW	LW	SW	LW	SW	LW	SW	LW
APRE, %	0.27	0.02	0.49	0.14	5.82	0.55	8.08	0.99	51.7	1.52	0.49	0.19
CPU, s	6.30	158.2	0.69	16.11	0.31	6.45	0.20	3.22	0.14	1.64	4.95	5.33

As can be seen from Table 4.1, among all the alternatives wavelength increment of 0.1 and variable wavelength increment provide higher accuracy with shorter computation time for both SW and LW ranges. However, computation times of wavelength increment of 0.1 was higher than that of variable wavelength increment so that variable wavelength increment seems to be the optimum alternative in terms of both computational efficiency and computational accuracy while running SBDART for the clear-sky atmosphere.

Calculations for cloudy sky atmosphere were carried by using a fixed cloud layer in between 1-2 km with a cloud optical depth of 60 and an average water droplet particle diameter 5.89 μm [8].

Table 4.2 displays the effect of wavelength increment on net fluxes for cloudy sky atmosphere. As can be seen from the table, variable wavelength increment is the optimum alternative for both computational efficiency and accuracy.

Table 4.2 Effect of wavelength increment (wl) on net fluxes for cloudy sky

	wl=0.01		wl=0.1		wl=0.25		wl=0.5		wl=1.0		vwl=0.01	
	SW	LW	SW	LW	SW	LW	SW	LW	SW	LW	SW	LW
APRE, %	0.45	0.01	0.70	0.14	7.15	0.37	14.80	0.75	55.91	0.70	0.45	0.09
CPU, s	6.39	160.8	0.69	16.13	0.28	6.44	0.20	3.31	0.16	1.64	5.03	5.39

4.3 Effect of Number of Streams on Computational Efficiency and Accuracy of SBDART

In order to evaluate the effect of number of streams on the predicted net fluxes in terms of computational efficiency and accuracy, SBDART was run for 4, 8 and 16 number of streams for SW range (0.2-4.0 μm) and LW range (4.0-100 μm) for both clear and cloudy sky atmospheres. The accuracy of net fluxes at any number of streams was evaluated by comparing it with the ones obtained with 32 streams.

Table 4.3 and 4.4 show the effect of number of streams on net fluxes for clear and cloudy sky atmospheres, respectively. As can be seen from the tables, the accuracy improves an order of magnitude with doubling the number of streams while the computation time does not change significantly. However, considering the time required to reach equilibrium temperatures when running the radiative code, optimum number of streams was selected to be 8 for both clear and cloudy atmospheres.

Table 4.3 Effect of number of streams (Nstr) on net fluxes for clear sky

	Nstr =16		Nstr =8		Nstr =4	
	SW	LW	SW	LW	SW	LW
APRE, %	0.0002	0.0011	0.0025	0.0319	0.0216	0.5010
CPU, s	7.61	8.59	5.31	6.03	4.95	5.33

Table 4.4 Effect of number of streams (Nstr) on net fluxes for cloudy sky

	Nstr =16		Nstr =8		Nstr =4	
	SW	LW	SW	LW	SW	LW
APRE, %	0.0018	0.0008	0.0436	0.0185	0.2004	0.4874
CPU, s	7.45	8.50	5.33	5.91	5.03	5.39

4.4 Effect of Presence of Cloud and CO₂ Concentration on Temperatures

In order to investigate the effect of CO₂ on atmospheric temperature changes, RCM4EAS developed in this study was used to predict the equilibrium temperatures of the atmospheric layers and the surface for both clear and cloudy sky conditions. Calculations were carried out by using variable wavelength and 8 streams for both SW and LW ranges in atmosphere up to 62 km [5].

Calculations regarding the CO₂ sensitivity analysis were carried out on a personal computer with Intel Core2 Duo 3.16 GHz processor having 1.93 GB of RAM.

Figure 4.2 shows comparison between the times required to reach surface equilibrium temperature for different time increments and ocean layer depths in clear sky atmosphere. As can be seen from the figure, ocean layer depth and time increment does not significantly affect the surface equilibrium temperature but the time required to reach it. The combination of reasonably large time increment (48 h) and thin ocean layer depth (12.5 m) provides computational efficiency with favorable accuracy compared to that of small time increment (3 h) and thick ocean layer depth (100 m). This is why a time step of 48 hours and ocean layer depth of 12.5 m were used in clear sky atmosphere.

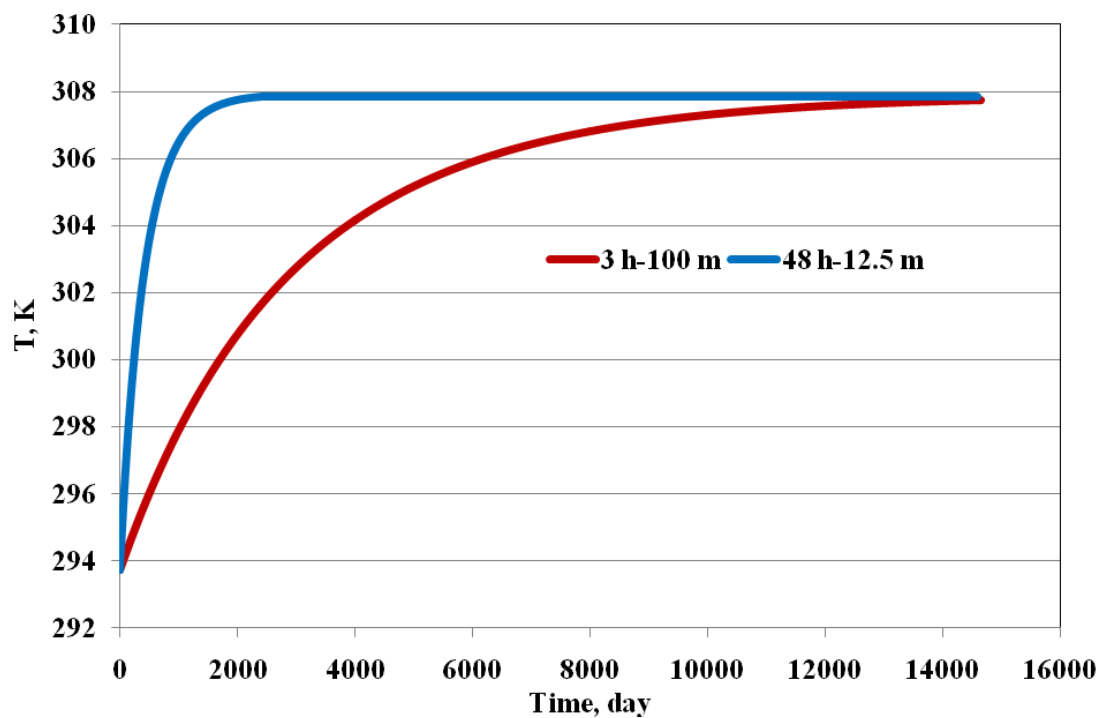


Figure 4.2 Surface temperatures with respect to time for different time increments and ocean layer depths in clear sky

Figure 4.3 shows the effect of doubling CO₂ concentration on surface temperature for clear sky condition. As can be seen from the figure, when CO₂ concentration is doubled, the equilibrium surface temperature increases by 4.2 K.

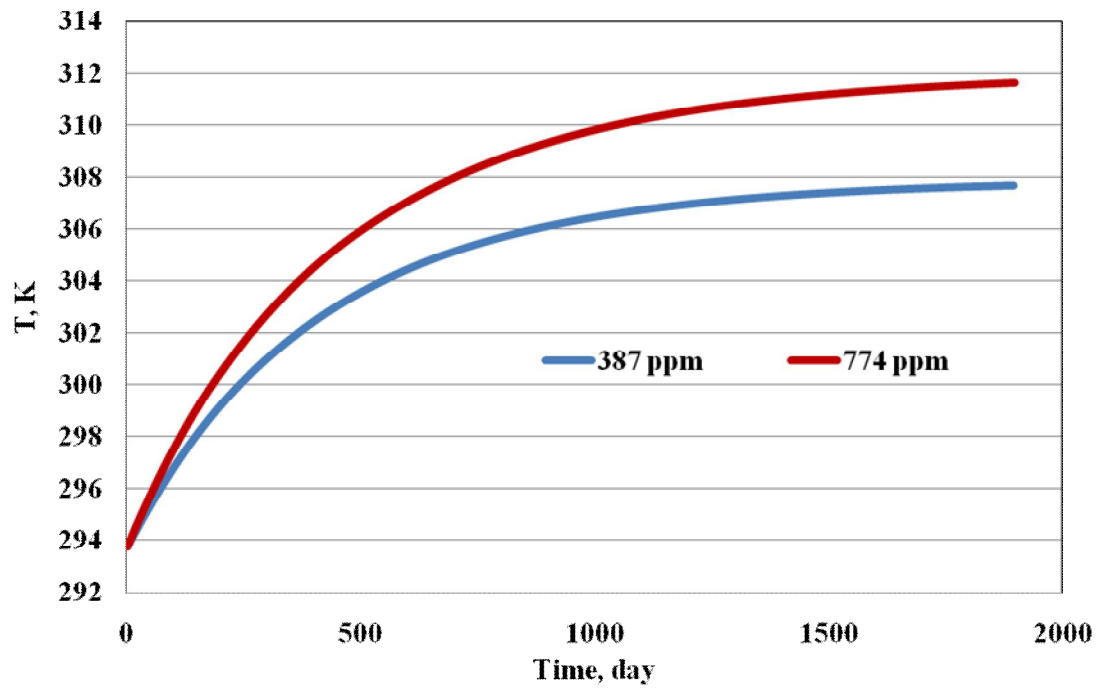


Figure 4.3 Surface temperatures with respect to time in clear-sky

For cloudy sky atmosphere, a typical cloud located within 2.5 to 3.4 km (approximately) with an average liquid water path of 40 g/m^2 and an average water droplet diameter of $10 \text{ }\mu\text{m}$ [11] was employed.

Figure 4.4 displays comparison between the times required to reach surface equilibrium temperature for different time increments in cloudy sky atmosphere. As can be seen from the figure large time increment (6 h) leads to instability and increases the time required to reach equilibrium. Therefore small time increment (3 h) was selected for the rest of the calculations.

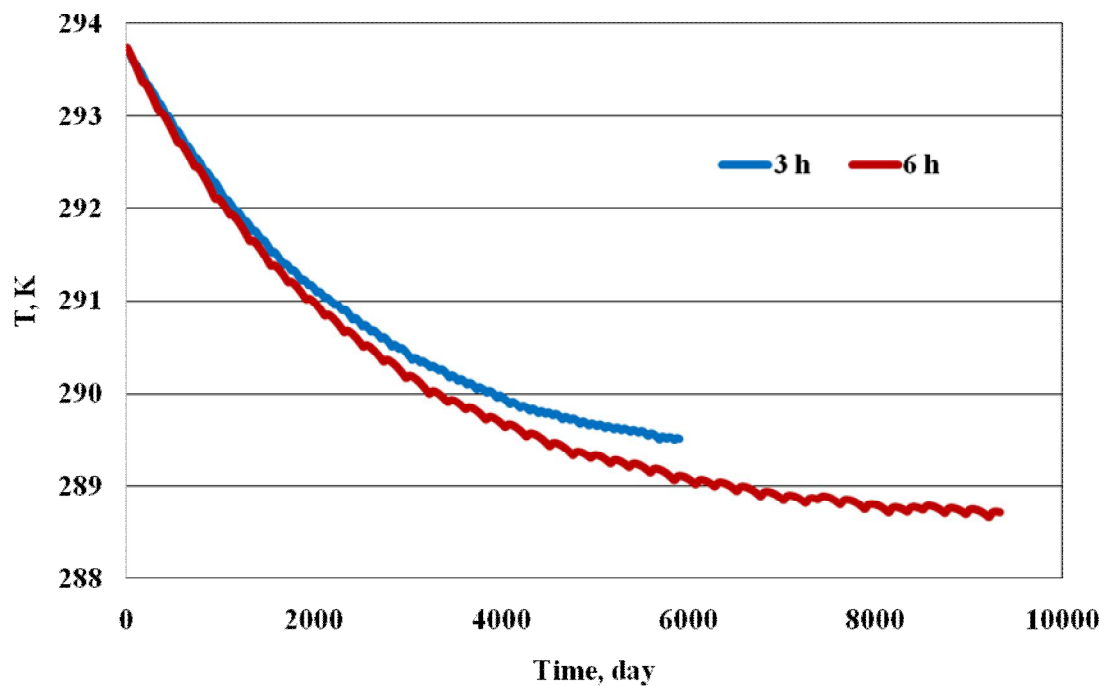


Figure 4.4 Surface temperatures with respect to time for different time increments in cloudy sky

Figure 4.5 illustrates the effect of doubling CO₂ concentration on surface temperature for cloudy sky atmosphere. Surface temperature was found to increase by 2.1 K when CO₂ concentration is doubled. It is worth noting that time required to reach the surface equilibrium temperature is approximately 6000 days during which all the other forcings except CO₂ are assumed to remain unchanged. Although the time required to reach equilibrium can be shortened by using an initial surface temperature closer to the equilibrium temperature, it still requires a considerable time period, over a year [7,25], during which all the other forcings except CO₂ are assumed unchanged. Therefore, it should be noted that this temperature increase reflects only the effect of CO₂ doubling and excludes the effect of other forcings which might positively or negatively affect this temperature increase.

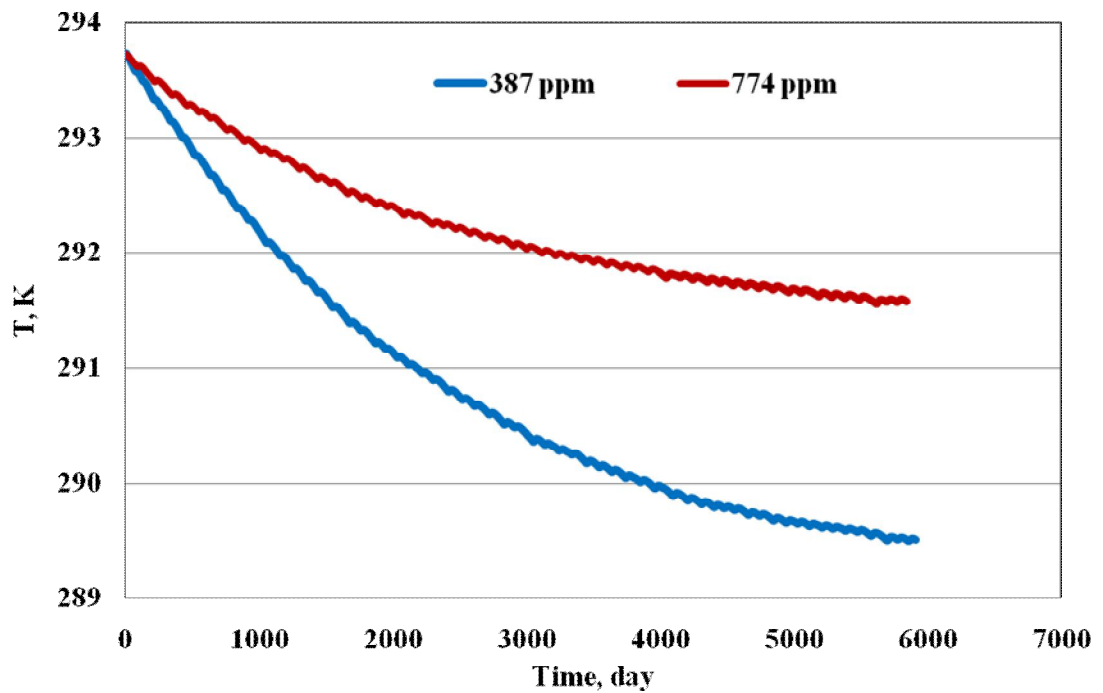


Figure 4.5 Surface temperatures with respect to time for cloudy sky

Figure 4.6 displays equilibrium temperature profiles for both clear and cloudy sky atmospheres for two CO₂ concentration levels. As can be seen from the figure, equilibrium temperature profiles up to 25 km are strongly affected by the presence of cloud irrespective of the CO₂ concentration level. At higher altitudes, however, the situation is reversed and temperature profiles are significantly affected by CO₂ concentration.

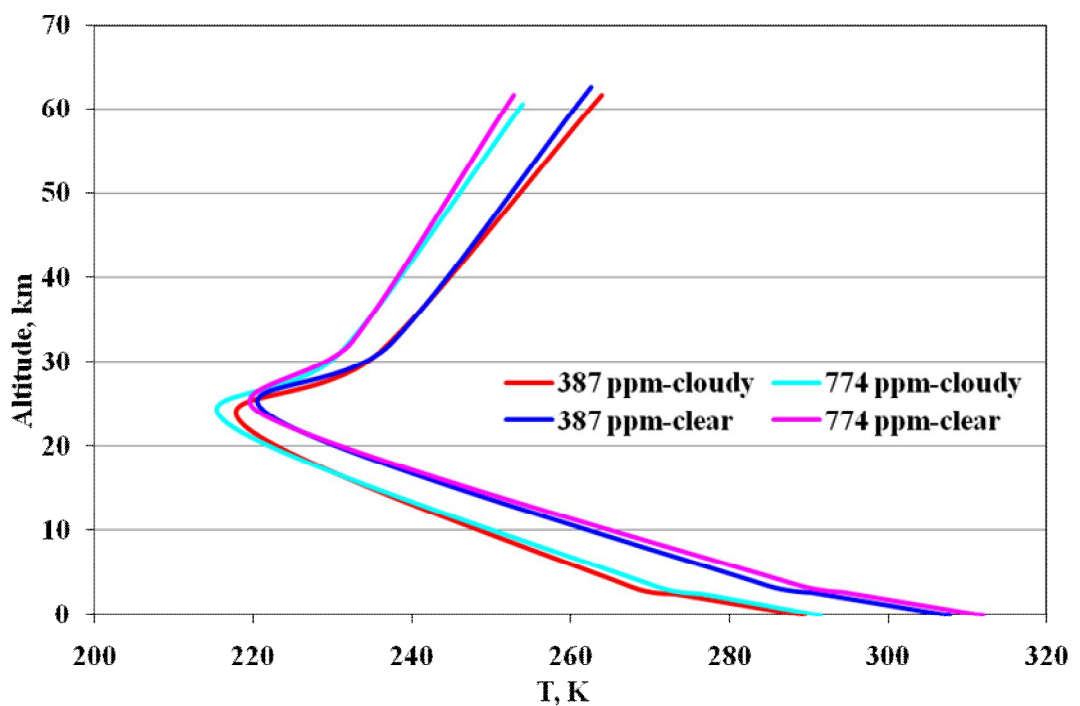


Figure 4.6 Equilibrium temperature profiles of clear and cloudy sky atmospheres

4.5 Comparison of Predictions by RCM4EAS and Literature

The code developed in this study was run by utilizing the same data employed by Hu et al. [11] and the predicted equilibrium surface temperatures for the cloudy sky atmosphere were compared with the available data in the literature.

The calculations were carried out for both SW (0.2-5.0 μm) and LW (4.0-100.0 μm) as opposed to 0.28-4.0 μm and 4.0-150.0 μm employed by Hu et al. [11] in atmosphere up to 62 km [5] containing 300 ppm CO_2 . Equilibrium surface temperatures obtained by this study and the study of Hu et al. [11] were found to be 288.8 K and 290 K, respectively. This favorable agreement points out the reliability of the code to be used for modeling of earth-atmosphere systems.

CHAPTER 5

CONCLUSIONS

In this thesis study, a 1-D radiative-convective model for the earth-atmosphere system (RCM4EAS) was developed for clear and cloudy sky conditions. Radiative component of the code is Santa Barbara DISORT (Discrete Ordinate Radiative Transfer) Atmospheric Radiative Transfer (SBDART). The code was used for the investigation of the effect of doubling CO₂ concentration on temperature profiles of the earth-atmosphere system. The following conclusions were reached under the observations of this study:

- SBDART is an accurate radiation code that can be used in radiative-convective modeling of the earth-atmosphere systems.
- Use of variable wavelength increment and eight streams in SBDART is recommended for the optimum accuracy and CPU efficiency when the code is coupled to a convective model.
- CO₂ sensitivity analyses revealed that doubling the CO₂ concentration in the earth's atmosphere from its present value (387 ppm) results in an increase in equilibrium surface temperature of 4.2 K in the clear sky atmosphere as opposed to 2.1 K in cloudy sky atmosphere with typical cloud physical parameters. It is worth noting that times required to reach equilibrium surface temperatures are approximately 2000 and 6000 days for clear and cloudy sky atmospheres, respectively and these temperature increases are calculated assuming that all the other parameters except CO₂ concentration remain unchanged within these time periods. Therefore, it should be noted that these

temperature increases reflect only the effect of CO₂ doubling and excludes the effect of other forcings which might positively or negatively affect these temperature increases.

- Comparison of equilibrium surface temperatures computed by the RCM4EAS with the ones reported in literature produces favorable agreement.
- Equilibrium temperature profiles up to 25 km are strongly affected by the presence of cloud irrespective of the CO₂ concentration level. At higher altitudes, however, temperature profiles are significantly affected by CO₂ concentration.

In conclusion, overall evaluation of the performance of the radiative-convective code developed in this study points out that it can be used with confidence in modeling earth-atmosphere system.

REFERENCES

1. Liou, K.N., An Introduction to Atmospheric Radiation, 2nd Ed., *International Geophysics Series*, Vol 84, Academic Press, San Diego, California, USA, 2002.
2. Aydın, G., Radiative-Convective Model for One-Dimensional Longwave Clear Sky Atmosphere, M.Sc. Thesis, Middle East Technical University, Turkey, 2008.
3. Möller F., and S. Manabe, Über das Strahlungsgleichgewicht in der Atmosphäre, *Z.f. Meteor.*, Vol 15 pp. 3-8, 1961.
4. Manabe S., and F. Möller, On the Radiative Equilibrium and the Heat Balance of the Atmosphere, *Mont. Weath. Rev.*, Vol 89 (12), 1961.
5. Manabe, S., and R. F. Strickler, Thermal equilibrium of the atmosphere with a Convective Adjustment, *J. Atmos. Sci.*, Vol 21 pp. 361–385, 1964.
6. Ramanathan, V., and J.A. Coakley, Climate Modelling Through Radiative-Convective Models, *Reviews of Geophysics and Space Physics*, Vol 16 (4) pp. 465-489, 1978.
7. MacKay R.M., and M.A.K. Khalil, Theory and Development of a One-Dimensional Radiative-Convective Model, *Chemosphere*, Vol 22 pp. 383-417, 1991.
8. Fu, Q., K.N. Liou, M.C. Cribb, T. P. Charlock, and A. Grossman, Multiple Scattering Parameterization in Thermal Infrared Radiative Transfer, *J. Atmos. Sci.*, Vol 54 pp. 2799–2812, 1997.
9. Toon, O.B., C.P. McKay, and T.P. Ackerman, Rapid Calculation of Radiative Heating Rates and Photodissociation Rates in Inhomogeneous Multiple Scattering Atmospheres, *J. Geophys. Res.*, Vol 94 pp. 16287–16301, 1989.
10. Liou, K.N., A Numerical Experiment on Chandrasekhar's Discrete-Ordinates Method for Radiative Transfer: Application to Cloudy and Hazy Atmospheres, *J. Atmos. Sci.*, Vol 30 pp. 1303–1326, 1973.
11. Hu, Y. and K. Stamnes, Climate Sensitivity to Cloud Optical Properties, *Tellus*, Vol 52B pp. 81-93, 2000.
12. Tsay S.-C., K. Stamnes, and K. Jayaweera, Radiative Energy Budget in the Cloudy and Hazy Arctic, *J. Atmos. Sci.*, Vol 46 (7) pp. 1002-1018, 1989.

13. Pierluissi, J.H., and G.-S. Peng, New Molecular Transmission Band Models for LOWTRAN, *Opt. Eng.*, Vol 24 (3) pp. 541–547, 1985.
14. Ricchiazzi P., S. Yang, C. Gautier and D. Sowle, SBDART: A Research and Teaching Tool for Plane-Parallel Radiative Transfer in the Earth's Atmosphere, *Bull. Am. Met. Soc.*, Vol 79 (10) pp. 2101-2114, 1998.
15. Wiscombe, W.J., Improved Mie Scattering Algorithms, *Appl. Opt.*, Vol 19 pp. 1505–1509, 1980.
16. van de Hulst, H.C., Asymptotic Fitting, A Method for Solving Anisotropic Transfer Problems in Thick Layers, *J. Comput. Phys.*, Vol 3 pp. 291–306, 1968.
17. Hansen, J.E., Exact and Approximate Solutions for Multiple Scattering by Cloudy and Hazy Planetary Atmospheres, *J. Atmos. Sci.*, Vol 26 pp. 478–487, 1969.
18. Wiscombe, W.J. and J.W. Evans, Exponential-Sum Fitting of Radiative Transmission Functions, *J. Comput. Phys.*, Vol 24 pp. 416–444, 1977.
19. Stamnes, K., S. Tsay, W. Wiscombe, and K. Jayaweera, Numerically Stable Algorithm for Discrete-Ordinate-Method Radiative Transfer in Multiple Scattering and Emitting Layered Media, *Appl. Opt.*, Vol 27 pp. 2502–2509, 1988.
20. Thekaekara, M.P., Extraterrestrial Solar Spectrum, 3000-6100 Å at 1-Å Intervals, *Applied Optics*, Vol 13 (3) pp. 518-522, 1974.
21. VanHoosier, M.E., J.D. Bartoe, G.E. Brueckner, and D.K. Prinz, Absolute solar spectral irradiance 120nm-400nm: Results from the Solar Ultraviolet Spectral Irradiance Monitor (SUSIM) experiment on board Spacelab 2, *Astro. Lett. and Communications*, Vol 27 pp. 163-168, 1988.
22. Neckel, H. and D. Labs, The Solar Radiation between 3300 and 12500 Angstroms, *Solar Physics*, Vol 90 pp. 205-258, 1984.
23. Wehrli, Ch., Extra-Terrestrial Solar Spectrum, Publication No. 615 July 1985, Physikalisch-Meteorologisches Observatorium and World Radiation Center, CH-7260 Davos-Dorf, Switzerland, 1985.
24. Tanre, D., C. Deroo, P. Duhaut, M. Herman, J. J. Morcrette, J. Perbos, and P. Y. Deschamps, Description of a Computer Code to Simulate the Satellite Signal in the Solar Spectrum: The 5S code. *Int. J. Remote Sens.*, Vol 11 (4) pp. 659–668, 1990.
25. Manabe, S., and R.T. Wetherald, Thermal Equilibrium of the Atmosphere with a Given Distribution of the Relative Humidity. *J. Atmos. Sci.*, Vol 24 pp. 241–259, 1967.

26. Stone, P.H. and J.H. Carlson, Atmospheric Lapse Rate Regimes and Their Parameterization, *J. Atmos. Sci.*, Vol 36 pp. 415-423, 1979.
27. National Oceanic and Atmospheric Administration, NOAA Research, <http://www.esrl.noaa.gov/gmd/ccgg/trends/>, last accessed date: 12/10/2010.
28. McClatchey, R.A., R.W. Fenn, J.E.A. Selby, F.E. Volz, and J.S. Garing, Optical properties of the atmosphere, AFCRL-72-0497, Air Force Cambridge Res. Lab., Bedford, Mass., 1972.
29. Stull, R.B., Static Stability-An Update, *Bull. Am. Met. Soc.*, Vol 72 (10) pp.1521-1529, 1991.
30. Chandrasekhar, S., Radiative Transfer, The International Series of Monographs of Physics, Oxford at the Clarendon Press, Oxford, UK, 1950.
31. Stamnes, K., and H. Dale, A new look at the discrete-ordinate method for radiative transfer calculations in anisotropically scattering atmospheres. II. Intensity computations, *J. Atmos. Sci.*, Vol 38 pp. 2696–2706, 1981.
32. Davis, P.F., and P. Rabinowitz, Methods of Numerical Integration, 2nd Ed., Academic Press, San Diego, California, USA, 1984.
33. Zdunkowski, W., T. Trautmann, and A. Bott, Radiation in the Atmosphere, Cambridge Univ. Press, Cambridge, UK, 2007.
34. Clough, S.A., M.J. Iacono, and J.-L. Moncet, Line-by-line Calculations of Atmospheric Fluxes and Cooling Rates: Application to Water Vapor, *J. Geophys. Res.*, Vol 97 pp. 761–785, 1992.

APPENDIX A

UTILIZATION OF LEGENDRE POLYNOMIALS IN RADIATIVE TRANSFER CALCULATIONS

The angular distribution of the scattered energy is represented by the phase function, $P(\mu, \varphi; \mu', \varphi')$, as a function of the scattering angle, Θ and considering spherical geometry, the scattering angle is related to the incoming and outgoing directions as:

$$\cos \Theta = \mu\mu' + (1 - \mu^2)^{1/2} (1 - \mu'^2)^{1/2} \cos(\varphi' - \varphi) \quad (\text{A.1})$$

Having unique mathematical properties, the Legendre polynomials have been used extensively in the analysis of radiative transfer problems. The phase function, P_l , may be expressed in terms of Legendre Polynomials as follows:

$$P(\cos \Theta) = P(\mu, \varphi; \mu', \varphi') = \sum_{l=0}^N w_l P_l \left(\mu\mu' + (1 - \mu^2)^{1/2} (1 - \mu'^2)^{1/2} \cos(\varphi' - \varphi) \right) \quad (\text{A.2})$$

where based on the orthogonality property, the expansion coefficient, w_i , is given by:

$$w_l = \frac{2l+1}{2} \int_{-1}^1 P(\cos \Theta) \cos \Theta \, d \cos \Theta \quad l = 0, 1, \dots, N \quad (\text{A.3})$$

$P(\mu, \varphi; \mu', \varphi')$ may be extended in a series of $2N$ Legendre polynomials by the addition theorem for spherical harmonics as in Eq. (A.4).

$$P(\mu, \varphi; \mu', \varphi') = \sum_{m=0}^{2N-1} \sum_{l=m}^{2N-1} w_l^m P_l^m(\mu) P_l^m(\mu') \cos m(\varphi' - \varphi) \quad (A.4)$$

$l = m, \dots, 2N-1$

Intensity and the source term may be expanded in a Fourier cosine series as:

$$I(\tau, \mu, \varphi) = \sum_{m=0}^{2N-1} I^m(\tau, \mu) \cos m(\varphi_0 - \varphi) \quad (A.5)$$

$$Q(\tau, \mu, \varphi) = \sum_{m=0}^{2N-1} Q^m(\tau, \mu) \cos m(\varphi_0 - \varphi) \quad (A.6)$$

Noting the orthogonality of associated Legendre polynomials, P_l^m , Eq. (3.29) turns into $2N$ independent equations inserting Eq. (A.4 to 6) as:

$$\mu \frac{dI^m(\tau, \mu)}{d\tau} = I^m(\tau, \mu) - \int_{-1}^1 D^m(\tau, \mu, \mu') I^m(\tau, \mu') d\mu' - Q^m(\tau, \mu) \quad (A.7)$$

$m = 0, \dots, 2N-1$

where

$$Q^m(\tau, \mu) = \frac{\omega(\tau) I_0}{4\pi} (2 - \delta_{m0}) \sum_{l=0}^{2N-1} (-1)^{l+m} (2l+1) g_l^m(\tau) P_l^m(\mu) P_l^m(\mu) e^{-\tau/\mu_0} + \delta_{m0} Q^l(\tau)$$

$$D^m(\tau, \mu, \mu') = \frac{\omega(\tau)}{2} \sum_{l=m}^{2N-1} (2l+1) g_l^m(\tau) P_l^m(\mu) P_l^m(\mu')$$

$$g_l^m(\tau) = \frac{(l-m)!}{(l+m)!} \frac{1}{2} \int_{-1}^1 P(\tau, \cos \theta) P_l(\cos \theta) d \cos \theta \quad \text{and} \quad \begin{cases} \delta_{m0} = 1 & \text{if } m = 0; \\ \delta_{m0} = 0 & \text{if } m \neq 0 \end{cases}$$

Similarly, bidirectional reflectivity, $\rho_d(\mu, \varphi; -\mu', \varphi')$, can be expressed in a series of $2N$ Legendre polynomials assuming that it is a function only of the angle θ between the incident and the reflected radiation given in Eq. (A.8).

$$\rho_d(\mu, \varphi; -\mu', \varphi') = \sum_{l=0}^{2N-1} (2l+1) h_l P_l \left(-\mu\mu' + (1-\mu^2)^{1/2} (1-\mu'^2)^{1/2} \cos(\varphi' - \varphi) \right) \quad (A.8)$$

Furthermore using the addition theorem for spherical harmonics,

$$\rho_d(\mu, \varphi; -\mu', \varphi') = \sum_{l=0}^{2N-1} \rho_d^m(\mu, -\mu') \cos m(\varphi' - \varphi) \quad (\text{A.9})$$

$$\rho_d^m(\mu, -\mu') = (2 - \delta_{0m}) \sum_{l=m}^{2N-1} (2l+1) h_l^m P_l^m(-\mu') P_l^m(\mu) \quad (\text{A.10})$$

where

$$h_l^m = h_l \frac{(l-m)!}{(l+m)!} \quad \text{and} \quad h_l = \frac{1}{2} \int_{-1}^1 P_l(\cos \theta) \rho_d(\cos \theta) d \cos \theta$$

Substituting Eq. (A.9) into Eq. (3.27) and using Eq. (A.5) results in the following form of RTE, Eq. (A.11), for the bottom boundary.

$$\begin{aligned} I^m(\tau_L, \mu) = I_g^m(\mu_i) = & \delta_{0m} \varepsilon(\mu) B(T_g) + (1 + \delta_{0m}) \int_0^1 \mu' \rho_d^m(\mu, -\mu') I^m(\tau_L, -\mu') d\mu' \\ & + \frac{\mu_0}{\pi} I_0 e^{-\tau_L/\mu_0} \rho_d^m(\mu, -\mu_0) \end{aligned} \quad (\text{A.11})$$

APPENDIX B

NUMERICAL SOLUTION PROCEDURE OF DISCRETIZED RTE

Represented for the upward and downward intensities separately, Eq. (3.32) for any layer in Fig. 3.7 can be given in the matrix form as the following:

$$\frac{d}{d\tau} \begin{bmatrix} I^+ \\ I^- \end{bmatrix} = \begin{bmatrix} -\alpha & -\beta \\ \beta & \alpha \end{bmatrix} \begin{bmatrix} I^+ \\ I^- \end{bmatrix} + \begin{bmatrix} \tilde{Q}^+ \\ \tilde{Q}^- \end{bmatrix} \quad (\text{B.1})$$

where

$$I^\pm = [I^m(\tau, \pm\mu_i)], \quad \tilde{Q}^\pm = M^{-1}Q^m(\tau, \pm\mu_i) \quad i = 1, \dots, N$$

$$\alpha = M^{-1}(D^+W - I), \quad \beta = M^{-1}D^-W$$

with

$$M = [\mu_i \delta_{ij}], \quad W = [w_i \delta_{ij}] \quad i, j = 1, \dots, N$$

$$D^+ = [D^m(\mu_i, \mu_j)] = [D^m(-\mu_i, -\mu_j)] \quad i, j = 1, \dots, N$$

$$D^- = [D^m(-\mu_i, \mu_j)] = [D^m(\mu_i, -\mu_j)] \quad i, j = 1, \dots, N$$

In order to solve the system of 2N-coupled ordinary differential equations, first homogeneous solution of Eq. (B.1), i.e. when $\tilde{Q} = 0$, must be obtained as in Eq. (B.2)

$$I^\pm = G^\pm e^{-k\tau} \quad (\text{B.2})$$

which requires solution of a standard algebraic eigenvalue problem of order $2N \times 2N$ with the eigenvalues, k , and eigenvectors, G^\pm , as:

$$\begin{bmatrix} \alpha & \beta \\ -\beta & -\alpha \end{bmatrix} \begin{bmatrix} G^+ \\ G^- \end{bmatrix} = k \begin{bmatrix} G^+ \\ G^- \end{bmatrix} \quad (\text{B.3})$$

The resulting equation, Eq. (B.3), can be solved as a standard eigenvalue problem as stated by Stammes et al. [31].

Since the intensity across the layer interfaces must be continuous, Eq. (3.32) must satisfy the continuity condition and the following boundary conditions as follows:

$$\text{(Upper BC)} \quad I_1^m(0, -\mu_i) = I_0^m(-\mu_i) \quad i = 1, \dots, N \quad (\text{B.4})$$

$$\text{(Continuity)} \quad I_p^m(\tau_p, \mu_i) = I_{p+1}^m(\tau_p, \mu_i) \quad i = \pm 1, \dots, \pm N; \quad p = 1, \dots, L-1 \quad (\text{B.5})$$

$$\text{(Lower BC)} \quad I_L^m(\tau_L, \mu_i) = I_g^m(\mu_i) \quad i = 1, \dots, N \quad (\text{B.6})$$

where

$$I_g^m(\mu_i) = \delta_{0m} \mathcal{E}(\mu_i) B(T_g) + (1 + \delta_{0m}) \sum_{j=1}^N w_j \mu_j \rho_d^m(\mu_i, -\mu_j) I^m(\tau_L, -\mu_j) + \frac{\mu_0}{\pi} I_0 e^{-\tau_L/\mu_0} \rho_d^m(\mu_i, -\mu_0)$$

Inserting Eq. (3.33) into Eq. (B.4 to B.6) and omitting the m -superscript gives the system of $(2N \times L) \times (2N \times L)$ linear algebraic equations to be solved in order to obtain $(2N \times L)$ unknown coefficients, C_{jp} , ($j = \pm 1, \dots, \pm N$; $p = 1, \dots, L$) [19] in Eq. (B.7 to B.9).

$$\sum_{j=1}^N [C_{j1} G_{j1}(-\mu_i) + C_{-j1} G_{-j1}(-\mu_i)] = I_0(-\mu_i) - R_p(0, -\mu_i) \quad (\text{B.7})$$

$i = 1, \dots, N$

$$\begin{aligned} \sum_{j=1}^N C_{jp} G_{jp}(\mu_i) e^{-k_{jp}\tau_p} + C_{-jp} G_{-jp}(\mu_i) e^{k_{jp}\tau_p} - C_{jp+1} G_{-jp+1}(\mu_i) e^{-k_{jp+1}\tau_p} + C_{-jp+1} G_{-jp+1}(\mu_i) e^{k_{jp+1}\tau_p} \\ = R_{p+1}(\tau_p, \mu_i) - R_p(\tau_p, \mu_i); \end{aligned} \quad (\text{B.8})$$

$i = \pm 1, \dots, \pm N; p = 1, \dots, L-1$

$$\sum_{j=1}^N [C_{jL} \gamma_{jL}(\mu_i) e^{-k_{jL}\tau_L} + C_{-jL} \gamma_{-jL}(\mu_i)] = \gamma(\tau_L, \mu_i) \quad (\text{B.9})$$

$i = 1, \dots, N$

where

$$\gamma(\tau_L, \mu_i) = \delta_{0m} \varepsilon(\mu_i) B(T_g) - R_L(\tau_L, \mu_i) + \frac{\mu_0 I_0}{\pi} e^{-\tau_L/\mu_0} \rho_d(\mu_i, -\mu_0) + (1 + \delta_{0m}) \sum_{j=1}^N w_j \mu_j \rho_d(\mu_i, -\mu_j) R_L(\tau_L, -\mu_j)$$

$$r_{jL}(\mu_i) = G_{jL}(\mu_i) - (1 + \delta_{0m}) \sum_{n=1}^N w_n \mu_n \rho_d(\mu_i, -\mu_n) G_{jL}(-\mu_n)$$